Pedro Miguel Tavares de Almeida

Master of Chemical and Biochemical Engineering

Cu(I)-based electrodes for glucose monitoring in biofermentation processes

Dissertation submitted in partial fulfillment
of the requirements for the degree of

Master of Science in
Chemical and Biochemical Engineering

Adviser: Claudio Ampelli, Full Professor, University of Messina
Co-adviser: Mário Eusébio, Assistant Professor, NOVA University of Lisbon

Examination Committee

Chair: Isabel Fonseca
Rapporteur: Svetlozar Gueorguiev Velizarov
Member: Mário Eusébio

FACULDADE DE CIÊNCIAS E TECNOLOGIA
UNIVERSIDADE NOVA DE LISBOA

October, 2019

Cu(I)-based electrodes for glucose monitoring in biofermentation processes

This document was created using the (pdf)LaTeX processor, based on the "novathesis" template[1], developed at the Dep. Informática of FCT-NOVA [2].
[1] https://github.com/joaomlourenco/novathesis [2] http://www.di.fct.unl.pt

Aos meus pais.

Acknowledgements

Firstly i want to thank to all the responsible ones from both countries that able me to make the connection. It was an experiment that would definitely mark my life. The main responsible were without a doubt Professor Isabel Fonseca and Professor Mario Eusébio from FCT-UNL, and Professor Claudio Ampelli, Professor Giovani Neri and Silvia Marini from UNIME. Fortunally this five individuals help me a lot in this journey but there is one person that i would like to present my sincerely "obrigado", which is Ana Dallot from FCT-UNL Mobility Division. From there numerous others help me through, such as Kove, João and Daniele Giusi who support me a lot on experimental section. Daniele Giusi performed all the samples and characterization procedure and pass the information to me. And of course the family/friends that support me close despite the many kilometers between us.

Find it.

Abstract

In this document, Cu_2O, was widely studied due to its amazing electrode properties that will be discuss later. It was modified a total of four sensors (SPCE-DropSens), despite that two of them (P25 and HS-1), due to lack of preparation method and characterization were not main focus. Nevertheless, NC-9 and NC-10 structured crystalline nanocubes were deeply worked on. Electrochemical tests were run in all four sensors.

The structured nanocubes previously referred, NC-9 and NC-10, present sizes of 150-200 nm and 200-900 nm, respectively. The size differences is the main justification of the following NC-10 results conclusions. It was visible the lixing of NC-10 modified sensor material to the solution, which were probably due to sort of adherent difficulties.

Cuprous oxide in cubic nanostructured material, NC-9, shown a sensitivity, which is the main parameter to characterize the sensor yield, of 840 $\mu A\ mM^{-1}\ cm^{-2}$. Comparing this value with others in the literature is a competitive value due to the simplicity of the process and the high sensitivity value. Likewise selectivity and repeatibility parameters were also consider good to probably proceed to further future work. The electrooxidation reaction of this sensor that spikes the current signal undergoes in absorption controlled reaction, against the others three sensors.

NC-10 electrochemical trials were performed, firstly CV test were successfully ran but later trials were no more consider viable due to the lixing phenomenon referred previously. That is the reason why it was not calculated NC-10 sensitivity.

Keywords: ethanol fermentation; glucose detection; Cu_2O based electrode

Resumo

Neste documento, Cu_2O, foi estudado como potencial sensor para detecção de glucose devido às suas extraordinárias propriedades de semiconductor. Foram modificados um total de quatro sensores (SPCE-DropSens) embora dois deles, (P25 and HS-1), por falta da metodologia de preparação e caracterização não foram o foco principal. Ao contrário destes NC-9 e NC-10 nanocubos estructurados de forma cristalina foram o foco deste trabalho. No entanto os testes electroquimicos foram corridos nos quatro sensores.

Os nanocubos estructurados referidos anteriormente, NC-9 and NC-10, revelaram na parte de caracterização tamanhos entre 150-200 nm e 200-900 nm, respectivamente. Esta diferença no tamanho foi considerada a principal justificação pelos resultados do sensor NC-10. Este sensor revelou visivelmente lixiaviação do material por dificuldade na aderência ao eléctrodo.

Óxido de cobre numa estructura de nano cubos, NC-9, apresentou uma sensibilidade, que é o principal parâmetro para caracterizar o rendimento de um sensor, de 840 $\mu A\ mM^{-1}\ cm^{-2}$. Após comparação deste resultado obtido com outros sensores da literatura conclui-se que este sensor possui capacidade competitiva a outros da literatura pela sua simplicidade no processo de preparação e resultado de alta sensibilidade. Para além deste resultado este sensor revelou também alta selectividade e repetibilidade. A reacção de electrooxidação é controlada por absorção ao contrário dos outros três sensores.

Os testes electroquímicos foram todos realizados para o sensor NC-10, começando por CV de maneira viável mas ao contrário dos resultados nos restantes testes. Estes resultados foram considerados, como referido anteriormente, pela lixiviação do material. É a razão pela qual não foi calculada a sensibilidade do sensor NC-10.

Palavras-chave: fermentação de etanol; detecção de glucose; Cu_2O eléctrodo

Contents

List of Figures

List of Tables

Glossary

biofuel	A biofuel is a fuel that is produced through contemporary biological processes, such as agriculture and anaerobic digestion, rather than a fuel produced by geological processes such as those involved in the formation of fossil fuels, such as coal and petroleum, from prehistoric biological matter. If the source biomatter can regrow quickly, the resulting fuel is said to be a form of renewable energy.
lignocellulosic biomass	Lignocellulose refers to plant dry matter (biomass), so called lignocellulosic biomass. It is the most abundantly available raw material on the Earth for the production of biofuels, mainly bioethanol. It is composed of carbohydrate polymers (cellulose, hemicellulose), and an aromatic polymer (lignin).
starchy crops	Starch-based feedstocks include grains, such as corn or wheat, and tubers such as (sweet) potatoes and cassava. These feedstocks contain long complex chains of sugar molecules. The starch can easily be converted to fermentable sugars. The sugar can then be converted to ethanol or drop-in fuels. The fibrous part of the plants (e.g. wheat straw or corn stover) can be converted to advanced biofuels.

Acronyms

CV	cyclic voltammetry
HPLC	high-performance liquid chromatography
KOH	Potassium hidroxide
NC	nano cubes
NIRS	near-infrared spec-troscopy
SEM	scanning electron microscopy
SPCE	screen printed carbon electrode
XRD	x-ray powder diffraction

Chapter 1

Introduction

This chapter contains motivation for the development of the dissertation in section 1.1, then it is approach the problem in section 1.2 and the contributions of the document in section 1.3. The section 1.4 presents methodical approaches followed, the section 1.5 the used tools for practical purpose and the last one 1.6 the document presentation structure.

1.1 Motivation

Bioethanol as been designated the "*fuel of the future*" by Henry Ford himself. Over the years revealed to be as one of the most promising biofuels [1]. Nowadays, is the most popular alcoholic biofuel currently available on the worldwide market. Processes with ethanol as a final product have been highly investigated day by day among diverse research centers. Due to its less toxicity, bioethanol fermentation is more sustainable than other alcoholic fuels productions [1–3].

Ehthanol is produced from renewable agricultural products like sugar and corn plantations avoiding the nonrenewable sources like petroleum. Therefore, ethanol is not only a less toxic fuel as also less toxic than other alcoholic fuels (biofuels), as the products of incomplete oxidation of ethanol (acetic acid and acetaldehyde) are more sustainable than the by-products formed from other alcoholic biofuels fermentation processes [1]. Despite the energy equivalent *(toe = 42 kilojoules from 1 ton of crude oil)* that ethanol can "generate" in comparison to

crude oils fuels is about 68%, it still is consider a significant value to put work on it and developing more efficient/controlled processes [1].

Nowadays, bioethanol is usually blended to gasoline in frames between 10% *(v/v)* and 85% *(v/v)* [1]. Recent years shown a bioethanol production of over 100 billion liters worldwide shown in **(Table 1.1)** which the majority of it is for fuel purposes with a share of about 75% [1, 4]. Due to this great demand that is continue arising in the last few years the feed-stocks use in bioethanol fermentation processes and the technologies involved have been seriously investigated to came in is prime.

Table 1.1: Worldwide ethanol production [4]

Billions of litters	**Region**
61	USA
30	Brazil
5	European Union
4	China
2	Canada
105	**World**

Sugar, starch crops and lignocellulosic biomass (LCB) feed-stocks group up as the sources of bioethanol worldwide production [3]. Although, there is a segmentation around the globe about the 1^{st} generation feed-stock used between sugar and starch crops. In countries like Brazil, Colombia and India it is dominant the use of sugarcane, while in United States, China and European Union it is mainly used corn [2, 3].

Sugarcane based processes along with corn are facing a problem. The increased demand in food due to the huge population expansion in the last decades. This leads to a high feed-stock price and by direct consequence a high ethanol price [2]. Adding the global debate of convert food in fuel. This limit the use of sugar and starch crops for ethanol industrial production. There is clearly a urge related to use LCB, 2^{nd} generation feed-stock, more frequently [2].

LCB based biofuels are generally those that came from either residues of forest management or waste recovered from 1^{st} generation feed-stocks themselves. It can be even provide from whole plant biomass [2]. This sources do not face the same problems described previously on 1^{st} generation feed-stocks. They can be much classified as "*waste*"material and therefore also a renewable source that not face any big ethical issue [2]. Lignocellulosic, as the name points out it is a composite compound with cellulose and lignin mainly in it own composition

bonded to each other in the plant cell wall [2].

LCB still can not face the demand of bioethanol worldwide due to some industrial complications such as the amount of energy required for the pretreatment station (as waste is required to separate the renewable part from the nonrenewable); several number of steps on overall conversion; too much diversity in the composition and nature of the LCB itsel; inevitability of all sugars ferment by natural microorganisms and sub products that act like inhibitors of the fermentation process. All this facts built up all the bottlenecks for not using LCB more often in bioethanol fermentation processes [1]. Unfortunately the yield of the process, using 1^{st} generation feed-stocks, is monstrously higher in comparison to bioethanol fermentation from LCB which built the main reason for only 3% of the worldwide fuel demand is from bioethanol 2^{nd} generation production process [2].

Independently of the feed-stock used the main process are always built by 3 major steps. First it is required to extract from the feed-stocks the solution containing fermentable sugars [1]. Then, intuitively occurs the fermentation of the sugars in to ethanol and for last is necessary to obtain a more pure separated and purificated solution of the ethanol. This last one usually by distillation rectification dehydration method [1]. One of the reasons for the amount of ethanol produced is so big it is because basically any sugar containing material can be converted, by fermentation, in ethanol [2].

In a more detailed description of the process present in **(Figure 1.1)** the biomass from any feed-stock source when reaches the ethanol plant is isolated in a warehouse. In there the conditions are kept in a way to prevent the start of the fermentation and bacterial contamination of the crops [1]. Through the pretreatment section, from the storage compartments, essentially are extracted carbohydrates or processed in a way which makes it more easily to reach in further steps [1]. Then the pre-treated feed-stock is hydrolyzed to convert into simple sugars. Then by adding the right nutrients and yeasts for the fermentation put in a batch operated reactor it can be start the process of ethanol production [1]. Continuous processes have also been shown to be effectively in order to increase productivity the yeasts. In this cases are recycled or immobilized to get a higher cell density while the reactor keeps getting fed and products extracted [1].

Usually are set parameters such as temperature around 25 and 30 degrees Celsius and it takes between 6h and 72 h to the end of the process [1]. The difference in time mainly goes to the composition of the hydrolysate, cell density and yeast species. The final medium contains around 8-14%*(v/v)* in ethanol, due to the inhibitor factor for higher concentrations to the yeast cells and consequently reducing there activities [1]. The purification process yields an azeotropic mixture

made up of 95,5% of ethanol been the rest of it water or "*hydrated*"ethanol is possible to further dehydrated and get a 99,6% ethanol solution. The *vinasse* as it is called the remaining medium from the distillation column can be volatilized to produce co-products [1].

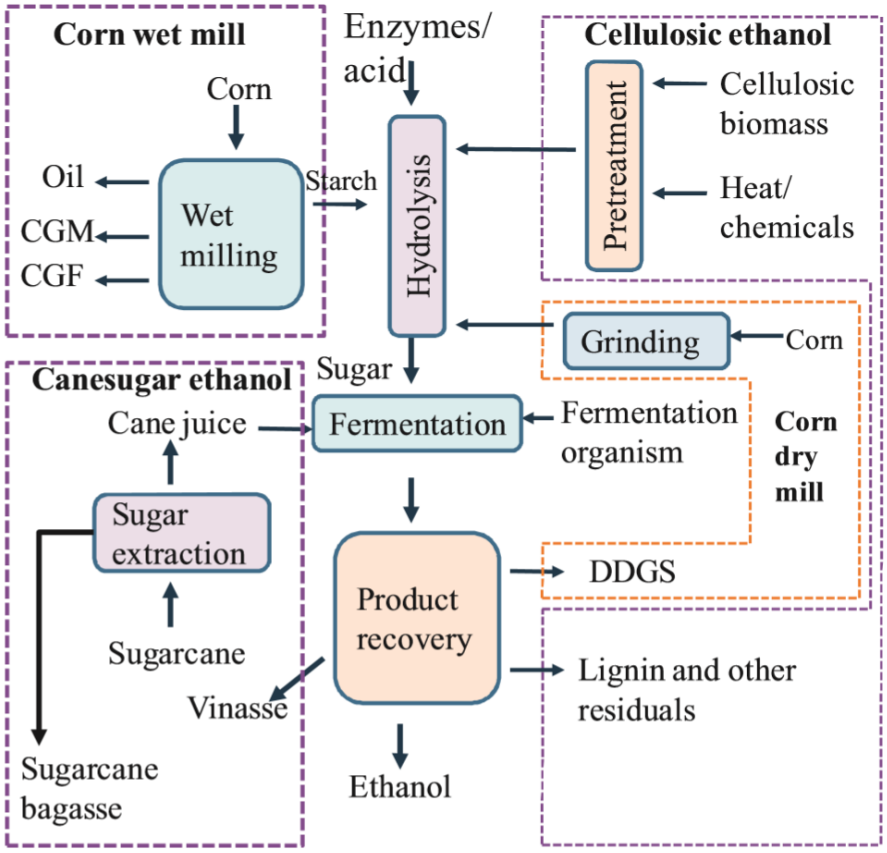

Figure 1.1: Schematic representation of ethanol production from different feedstocks [1]

Despite that the first two consider 1^{st} generation ethanol production sources are relatively more easy processes to handle. They still arise concerns surrounding material raw cost, environment awareness and a much more ethical question of wasting "food" to produce fuel [3]. That is why LCB (2^{nd} generation ethanol production normally from waste matter) has been recently researches focus on bioethanol production [3]. Although is necessary to keep in mind bioethanol production from this source still face some commercial barriers techniques that cannot compete and face economic fairness in comparison with the other two sources [3].

The control of the process is crucial to obtained a maximize yield in this reactions. By controlling something like the substrates concentration over time is possible to guaranteed a more efficient process. Using electrochemical sensors

adequate for glucose detection it is possible to control this parameters and guaranteed a more yield industrial process. The constant urge in get things to the nanoscale major due to environmental awareness has revealed amazing materials, technologies and processes over the last years. Which led to promising results in the electrochemical sensors field. The low cost and high efficiency acquired for this problem became a reality much needed. Day by day appears a new proposal of a material to modify the electrodes on an electrochemical sensor to undergo a certain electrocatalytic reaction to monitoring some analyte. In this work was developed a sensor for glucose detection in presence of other sugars and ethanol itself in medium. Therefore these analytes will not affect the electro activity perform of the sensor.

1.2 Problem

The main fuel sources are facing a depletion era which will lead to it extinguish. Actually this is predicted in 40-50 years [1, 2]. Fossil fuel sources made up to 80% of global energy demand which 58% of the total is use in transport section [2, 3].

With the world mostly dependent on getting energy by burning fossil fuels, such as oil, coal and natural gases it comes out 3 major points to notice [2, 5]. The first previously indicated is the fast depletion of this non renewable fossil fuels sources due to the exponential industrialization in the last decades globally speaking [2, 5]. In second it is important to point out the amount of greenhouse effect consequent from the daily use worldwide of this fuels. Such as carbon dioxide and much more non sustainable compounds that are release to the atmosphere and environment [2, 5]. Thirdly, the arise of the Middle East political crisis resulting in disruption of oil supply by one of the most powerful fuel sources of the world in the 1970s [2, 5]. This last one led to the global awareness of how dependent of fossil fuels we were 50 years ago and probably much more nowadays. Which allowed nations to met together to discuss more alternative paths then others fossil fuels in order to provide enough energy that is constantly demand [2, 5].

The constant global *"human footprint"* awareness that is exponentially increasing in late years made researchers look for tremendous paradigm shift renewable resources. Carbon emission **(Figure 1.2)** are from far the critical situation that industry faces [1]. The global goal of reducing this stat by 80% (v/v) came as a spotlight, focusing all directions in sustainable sources like biofuel, solar, wind and others [1]. Preventing further development of events such as global warming, acid rains and urban smog that earth already relays [1]. Currently ethanol reduces

greenhouse gas emissions by 43%, With the goal of achieving 50% in 2022 and even later 76% in the next decades [6].

A study from 2005 where it is compared the ethanol carbon dioxide emissions from sugar crops conclude that starch crops and fossil sources shown an amazing result of fifty times less carbon emissions from the renewable sources in comparison to the non renewable ones [6]. Although carbon dioxide is not the only greenhouse gas freighting which built the 43% shown previously [6].

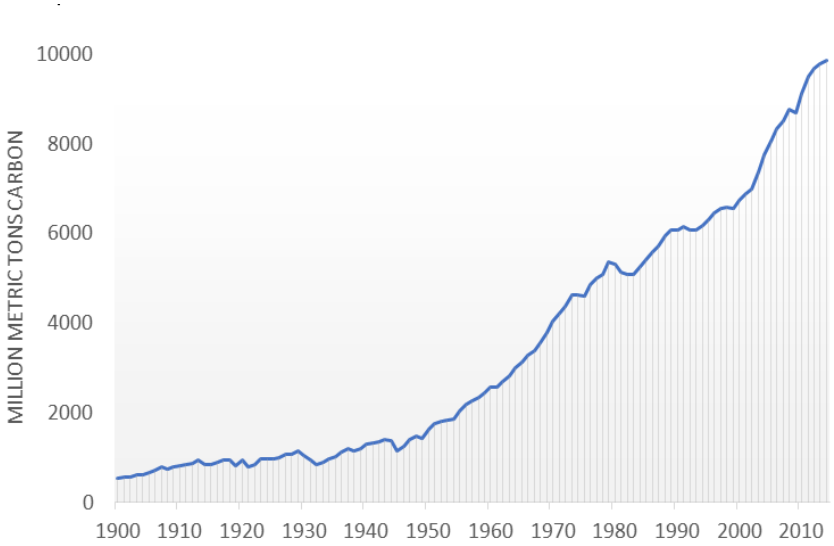

Figure 1.2: Worldwide carbon emission over the years [7]

1.3 Contributions

This master thesis posses several contributions, mainly from:

- Literature revision about all the subjects referred such like bioethanol production, ethanol fermentation process and electrochemical sensors fundamentals.
- Comprehension and practice of software/setup required for electrochemical sensor experiments.
- Preparation and characterization of the materials.
- Modification of screen-printed electrochemical sensors.
- Electrochemical trials about sensor glucose detection.

1.4 Methodic approaches

1.4.1 Development Steps

- Problem and motivation identification.
- Literature reading about bioethanol process and electrochemical sensors experimentation.
- Define master thesis purposes.
- Evaluation of the samples properties to sensing activity.
- Preparation of the sensors.
- Electrochemical experiments.
- Document writing and revision.

1.4.2 Searching and References Criteria

References used were search using Google Scholar as monitor tool, dialing key words like *"electrochemical sensors"*, *"glucose detection"*, *"ethanol fermentation"*, *"bioethanol production"*, not limiting the released year initially. Primary selection came from title, abstract and subject; further references were chosen by related authors.

These criteria shown up many sources mostly from the last decade by filtering for relevancy. Although some of the literature where was taken definitions for the theoretical introduction section did not require recent documents. Since are fields well known nowadays and with no updates to add. For example, ethanol fermentation, electrochemical tests and bioethanol production fundamentals are subjects set back then. Recent studies were used to establish the efforts and point we at as shown in **(Figure 1.3)**.

It is possible to separate this document in two time frame section, chapter 1 and chapter 2 with older literature reviews where is more about fundamentals definitions, due to the previous justification. And then, chapter 3 and chapter 4 with recent review literature, since they focus more on recent updates in sensor fields which is the case of state of art where there is not much interested in older discoveries.

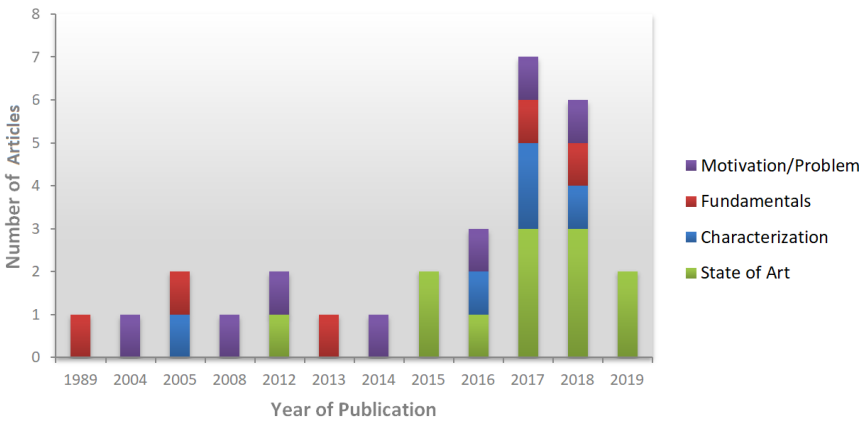

Figure 1.3: Time frame of literature

1.5 Used Tools

All the software (Originpro and Dropview), also electrochemical sensor set up were provided by the lab.

1.6 Document structure

The document presents the following structure:

- *Chapter 2* retains the fundamental concepts to understand all the theoretical behind the write of this document. Mainly required to advanced to the experimental procedures. Three focus were deeply studied, semiconductors and electrodes knowledge, characterization techniques and electrochemistry.
- *Chapter 3* reviews all the adequate literature for better comprehension of the thesis field and therefore have a comparative result for the final sensor trials. Firstly were taken a general fermentation sensor application and then were specify the type of fermentation, ethanol, and the analyte detected, glucose.
- *Chapter 4* is about the bulk preparation and characterization of the materials used on the electrodes and consequently ran in the electrochemical tests.
- *Chapter 5* describes all the electrochemical activity performed for the two main sensors prepared, along with the results obtained.
- *Chapter 6* resumed the main results obtained and where was compared with literature values. Also, possible future work by the team was described in this chapter.

This structure allows the reader to better understand the subject here exposed. Starting in better comprehension of the problem and some fundamentals concepts before dig in more technical/experimental lecture. Finally, is presented a conclusion and future work proposals.

Chapter 2

Fundamentals About Electrodes

In this chapter are exposed the fundamentals of electrodes, necessary for comprehension of this work. Firstly, in section 2.1 atomic structure and conduction/valence band relation are briefly resumed with crystal structure. Posterior detailed and mathematical exposed of characterization techniques on previous referred parameters are present in section 2.2.A explanation in section 2.3 of the electrochemical tests used to get the results present in this dissertation.

2.1 Electrode Structural Properties

2.1.1 Atomic Structure

Borh model shows a *"discontinued"* structure where it is possible to differentiate each band around atom nucleus. This allowed to better comprehension of electrons moving to higher or lower energy states. Those events are designate by excitation or decay movements, respectively. The nearest non-filled band is called conduction band [8]. In certain cases, can occur electron transitions between valence and conduction ones [8]. The hollow space (band gap) in which these are separate determinate if an element/compound is conductor or insulator [9]. Overlap of this two bands will lead to a conductor material or a metal; small gap are typically semiconductors and large one characterizes insulators [9]. Providing enough energy to overcome this gap is required to allow the transition [9].

In the characterization section will be crucial the perception of electronic band structure to correlate with a certain extent the optical properties of the materials. Both pictures in **(Figure 2.1)** show a drawn horizontal dashed line which meant to be the chemical potential. In **(Figure 2.1a)** the valence band (the bold one) is subtend to be completely field with electrons and therefore there is a gap with the next band (conduction band) which means insulator. Only with a certain amount of energy is allow the transition between bands. The fact that the maximum valence band and minimum conduction band are both at the same crystal momentum k subtends a direct band gap in the boundary zone.

Otherwise in **(Figure 2.1b)** where occurs overlap of the valence and conduction bands (therefore conditioning the two bands to share the electrons) getting both partially field providing the material metal properties. Although, if both bands were separated enough to get conduction band out of boundary zone it would be reach an indirect band gap. In this case the maximum valence band would no longer stand at the center of the figure and the minimum conduction band in the center of the figure would no more share the same k value.

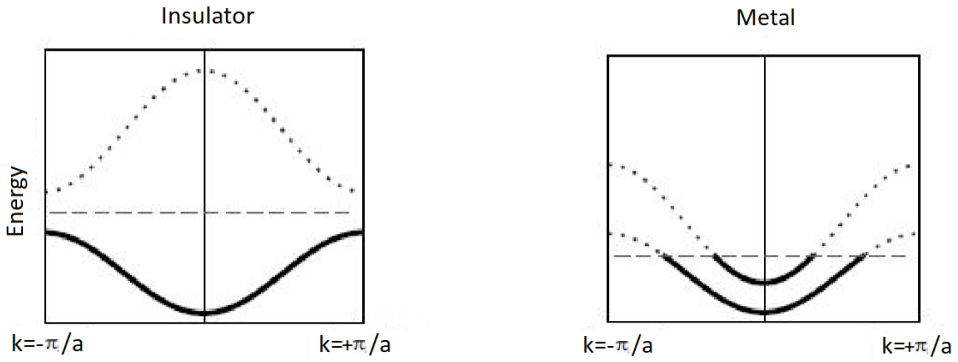

a) Insulator energy vs wave-vector with Fermi level

b) Metal energy vs wave-vector with Fermi level

Figure 2.1: Energy vs wave-vector with Fermi level (conductor and insulator distinction) [9]

Certain cases like in **(Figure 2.2)** both transitions are available in the same material (direct and indirect gaps are visible) for example in this case it is noticeable that the minimum energy excitation value goes to the indirect transition. This transition possess a change of crystal momentum value [9]. In other words the electron gets excited from the maximum of the valence band and the minimum of conduction band at different k. Despite the lower excitation energy it is very hard to occur an indirect transition by simply expose the system to light.

Energy momentum conservation it is a big deal in this matter. If a photon is

absorbed by the material, the compound get influence by both energy and momentum parameters. From the formula $h|k| = E/c$ where h is the Planck constant, k is the wave-vector, E is the energy of the photon and c the photon velocity (which get the value of the speed of light) the value of k output is really small due to the large value of the speed of light [9]. That means the system would not be able to conserve the momentum while exciting an electron across an indirect band gap. While the system can be exposed to photons with greater energy than the band gap, the system itself will find a disorder way to conserve crystal momentum via "*disorder assisted*"process. Which is basically a turn off on the perfectly periodical properties allowing the non perfectly conservation of the momentum. This phenom provides conditions to have some indirect transitions between the valence and conduction band [9].

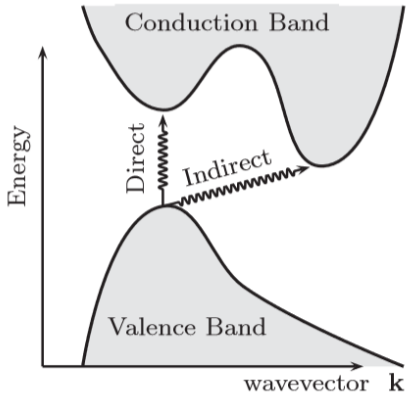

Figure 2.2: Energy vs wave-vector with Fermi level (direct and indirect transition distinction) [9]

With metals it is observed a more shiny object surface or material than insulators. This, is due to their highly conductivity. Photons excite electrons on the surface of the metal and re-emit light. Noble metals like gold silver and platinum are particularly more bright than others due to the non capability of forming insulating oxides when exposed to air like sodium does [9].

Comparing even between the metals group they have different colours from the reflected light. For example silver is much brighter than gold or copper. This last ones a more yellowish tonne because the band of silver is much more wide than the other two. The wider band allows photons in the blue and violet spectra be reflected, in opposition of gold and copper materials. Is also the explanation why silver approximates so close to a mirror because it reflect all visible light spectrum electrons, capturing the essence of reality [9].

2.1.2 Crystal Structure

Generally semiconductors used in sensor fields are presented in a crystalline form. Therefore, understanding the fundamentals about crystalline structure was crucial to further characterization of the compound [8]. Crystal structure which is basically the arrangement of the atoms in space are mostly reduce to one minor, a unit cell, **(Figure 2.3)**.

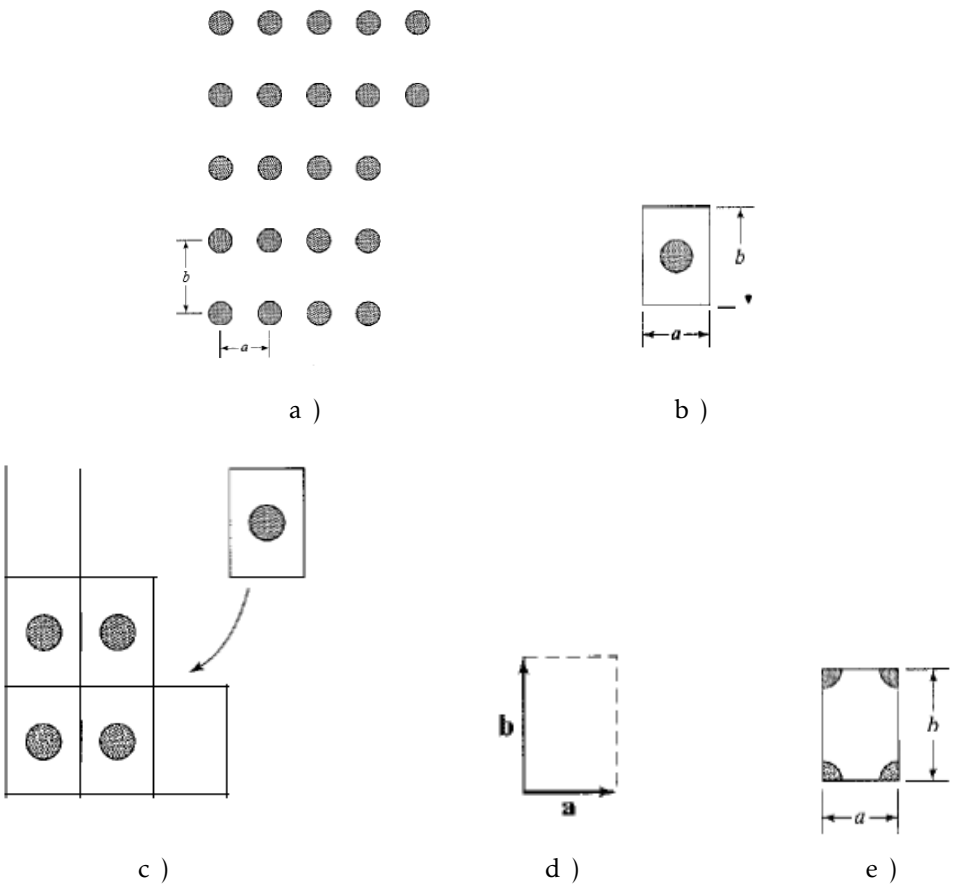

Figure 2.3: 2D unit cells schematic: a)Sample two-dimensional lattice; b) Unit cell corresponding to the part a) lattice; c) Reproduction of the original lattice; d) Basis vectors; e) An alternative unit cell [8]

These unit cells present in **(Figure 2.3b)** at two dimensional interface across combinations of assembles possibly to perhaps constitute a picture of how the compound looks like. Unit cells acts like building blocks to create a coherent structure between them. By fixing basic vectors **(Figure 2.3d)**, it is possible to get the vector across any two points in the crystalline structure. The vector is built from the formula $r = ha + kb$, where h and k are both integers. Nevertheless, in **(Figure 2.3b)** is not the only two dimensional lattice. In fact in **(Figure 2.3e)** shows a alternative organization of the atoms to became a different unit cell.

In certain situations, unit cells have advantageous to be set slightly larger then primitive unit cell (with the smallest size possible). This is reflected in orthogonal kind of structures. These non-cubic structures are more difficult to describe and visualize if using a primitive unit cell [8]. While two dimensional lattices help to get the fundamentals about the semiconductor structure, it is not enough to approach the three dimensional crystalline structure of the material. In **(Figure 2.4a)** is picture the simplest three dimensional unit cell, which is called simple cubic unit cell. This unit cell arrange eighth atoms in a way that only 1/8 of each are present in the unit cell itself like in **(Figure 2.4b)**. Again by translation and repping of this unit cell by the formula $r = ha + kb + lc$, where h, k and l are all integers it is obtained the other two three dimensional lattices shown in **(Figure 2.4c** and **Figure 2.4d)**.

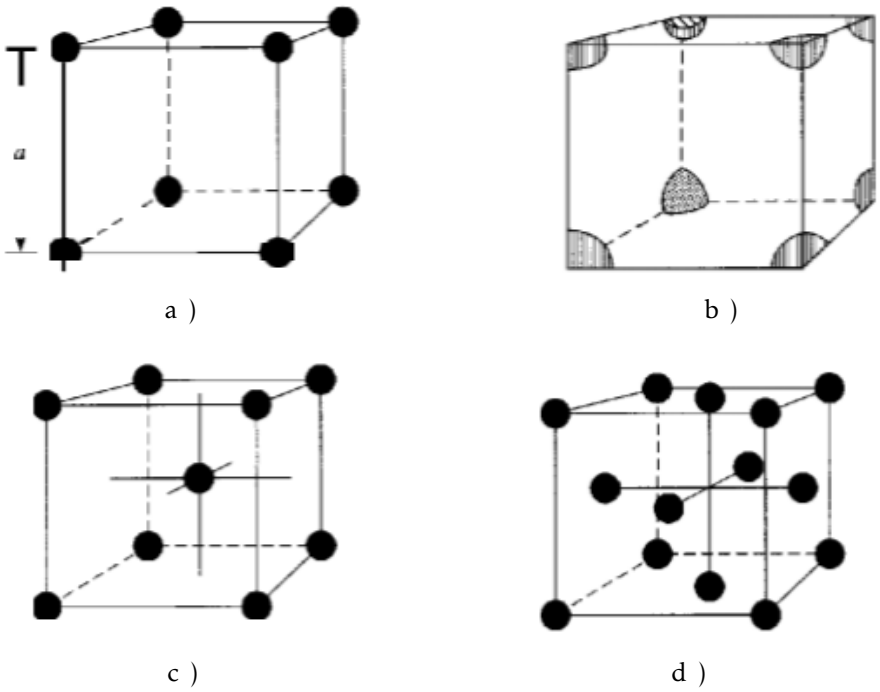

Figure 2.4: Simple three-dimensional unit cells: a) Simple cubic unit cell; b) Pedantically correct simple cubic unit cell including only the fractional portion of each corner atom actually within the cell cube. c) Body-centered cubic unit cell; d) Face-centered cubic unit cell [8]

In 1840's Bravais shown that this atoms distribution can be nominate in a limited number of lattices. In fact there are only a quite number of it [8]. Part of them are obviously the three lattices shown before in **(Figure 2.4)**, simple cubic, body-centered cubic and face-centres cubic unit cells. The 14 Bravais lattices can be observed in the **(Figure 2.5)**.

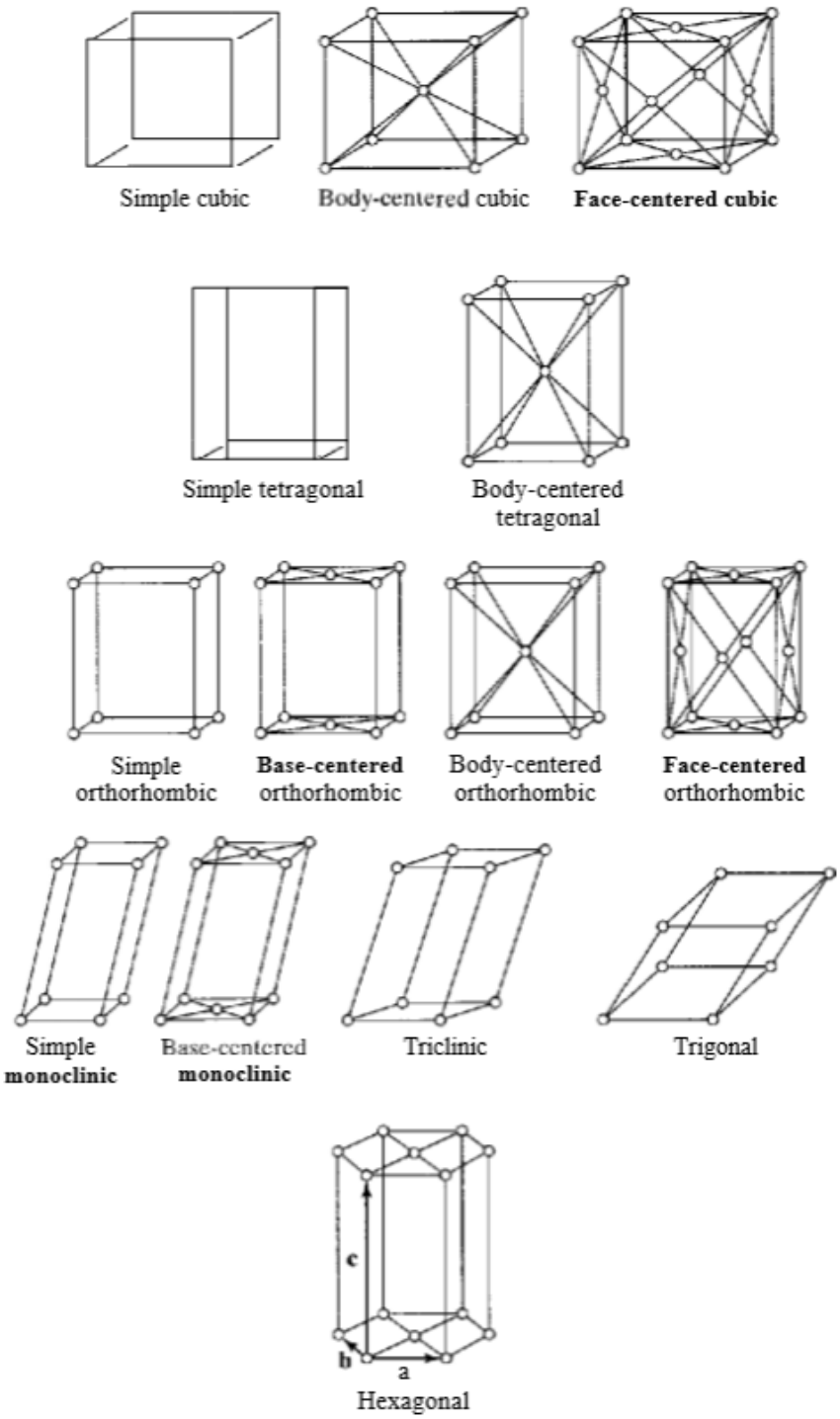

Figure 2.5: The 14 Bravais lattices [8]

Although, Bravais lattices can not built up all combinations when the subject is real crystals. In this cases where there are a huge number of atoms or molecules, there is an increase in the number of possible combinations by taking into account geometrical properties of them [8]. Much likely semiconductors the classification should be focused not on Bravais lattices, but on the symmetry characteristics exhibited by the crystal. Such as n-fold rotation symmetry, plane of symmetry, inversion center symmetry and rotation-inversion symmetry, denominated in **(Table 2.1)** along with **(Figure 2.6)**.

Table 2.1: The seven crystal systems

System	Characteristic Symmetry Element[1]	Bravais Lattice	Unit Cell Characteristics
Triclinic	None	Simple	$a \neq b \neq c$ $\alpha \neq \beta \neq \gamma \neq 90^o$
Monoclinic	One 2-fold rotation axis	Simple Base-centered	$a \neq b \neq c$ $\alpha = \beta = 90^o \neq \gamma$
Orthorhombic	Three mutually perpendicular 2-fold rotation axis	Simple Base-centered Body-centered Face-centered	$a \neq b \neq c$ $\alpha = \beta = \gamma = 90^o$
Tetragonal	One 4-fold rotation axis or a 4-fold rotation-inversion axis	Simple Body-centered	$a = b \neq c$ $\alpha = \beta == \gamma = 90^o$
Cubic	Four 3-fold rotation axis (cube diagonals)	Simple Body-centered Face-centered	$a = b = c$ $\alpha = \beta == \gamma = 90^o$
Hexagonal	One 6-fold rotation axis	Simple	$a = b \neq c$ $\alpha = 120^o$ $\beta = \gamma = 120^o$
Trigonal (Rhombohedral)	One 3-fold rotation axis	Simple	$a = b = c$ $\alpha = \beta = \gamma \neq 90^o$

Despite the fact for this work was not required Bravais lattices characterization of the crystalline structure, Miller indices were crucial to identify planes and directions [8]. This integer numbers are established in a manner analogous to the way vectors are usually nominated. A much more intuitive way. Miller indices can be easily obtained by following straightforward a step by step procedure. The four easy steps procedure shown in **(Table 2.2)** using as example **(Figure 2.7)**. There are still certain cases that need to be point out, in order to complete the description of the plane-indexing procedure [8].

(i) In case of a plane stands in a parallel to one of the three axis, the interception along that axis is taken to infinity. For example the plane shown in **(Figure**

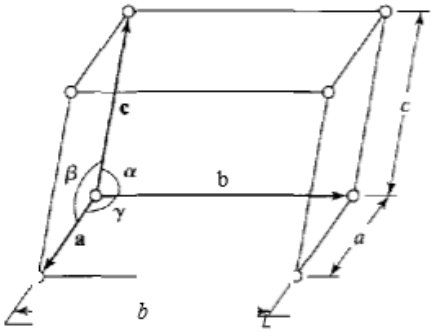

Figure 2.6: Definition of the angles and unit-cell dimensions cited in **(Table 2.1)** [8].

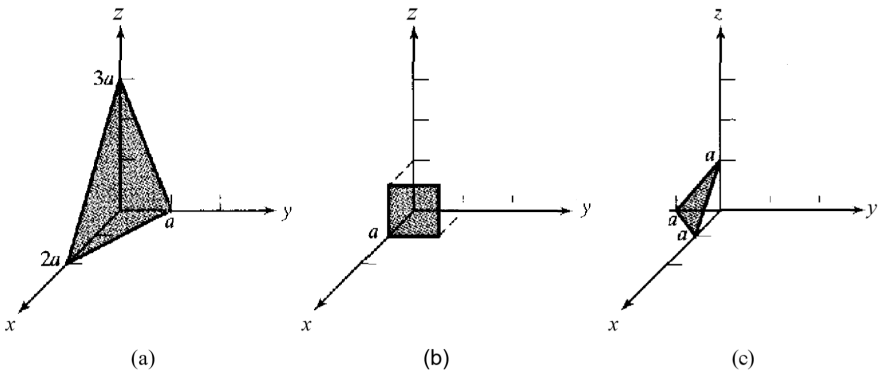

Figure 2.7: Sample cubic crystal planes [8]

Table 2.2: Miller index procedure for planes [8]

Indexing Procedure for Planes	Sample Information
(1) Divide each intercept value along the three axis by the unit cell length and recording those outputs numbers to obtain the pre-numbers.	2,1,3
(2) Invert those pre-numbers.	$\frac{1}{2}, 1, \frac{1}{3}$
(3) Use the minimum multiple number so the result in (2) get all integer numbers.	3,6,2
(4) Enclose the whole number set in curvilinear brackets.	(362)

2.7**b)**) intercepts the coordinate axis at 1, sub intending the other two axis are both taken to infinity and therefore it is designated the (100) plane [8].

(ii) If the plane intercepts an axis on a negative coordinate of it, a minus sign it is surplus on the Miller index designation. Is the case of **(Figure** 2.7**c))**, which is nominate the $(1\bar{1}1)$ plane [8].

(iii) All planes which fold in each other across a n-fold rotation axis are therefore consider equivalents and notated by {}. For example in **(Table** 2.1**)** if it is consider the cubic system is easily identify the six equivalent planes, (100), (010), (001), $(\bar{1}00)$, $(0\bar{1}0)$ and $(00\bar{1})$, which are collectively represented in Miller index as {100} planes [8].

(iv) Any plan cannot pass through the origin of coordinates, so it must be translate to other lattice point and then designated in case of interception [8].

2.2 Characterization Techniques

2.2.1 X-ray Powder Diffraction

X-ray powder diffraction (XRD) allows the characterization of nanoparticles composition and crystalline [10]. XRD plots data interpretation (intensity vs incidence angle) can lead to conclusion on the Miller indices and possible structure perception [10]. It is the Braggs Law **(Equation** 2.1**)** that correlates the results values from XRD to special disposal due to the following equations [8].

$$d = \frac{\lambda}{2sin(\theta)} \tag{2.1}$$

d = interplane spacing (nm)
λ = x-ray wavelength (nm)
θ = x-ray incidence angle (°)

The next **(Equation** 2.2**)** convert the interplane spacing calculated above in to Miller indices.

$$d_{h,k,l} = \frac{a}{\sqrt{h^2 + k^2 + l^2}} \tag{2.2}$$

$d_{h,k,l}$ = interplane spacing (nm)
a = unit cell dimension (nm)
h, k, l = Miller indices (integer)

2.2.2 UV-visible Diffuse Reflectance Spectroscopy

This method evaluates the material optical properties by emitting photons throw a previously select spectral range in to the sample [10]. In order to obtain bandgap energy from **(Equation 2.3)**, it is applied UV-visible diffuse reflectance spectroscopy technique [11]. Literature review correlates this property with absorbance by the next formula [11].

$$ahv = A(hv - E_g)^n \tag{2.3}$$

a = absorption coefficient
h = Plank constant (eVHz-1)
v = frequency (Hz)
A = frequency-independent constant
E_g = band gap energy (eV)
n = index of refraction **(Table 2.3)**

Table 2.3: Index refraction according to different band gap types [11]

Index od refraction	Band gap
$\frac{1}{2}$	Direct allowed transition
$\frac{3}{2}$	Direct forbidden transition
2	Indirect allowed transition
3	Indirect forbidden transition

Using Tauc plot (F(R) vs hv) extrapolating the linear region of the curve to intercept the x axis (photon energy) is possible to get the value of band gap energy E_g [11]. The absorption coefficient was evaluated by the Kubelka-Munk function (K-M, **Equation 2.4**), which correlates it to the reflectance obtained with this method [11].

$$a = \frac{(1 - R^2)}{2R} \tag{2.4}$$

a = absorbtion coefficient
R = reflectance

2.2.3 Scanning Electron Microscopy

Scanning electron microscopy (SEM) produces images of a certain sample, by shooting a focused beam of electrons on the compound surface. The name come after the idea of scanning the material using this type of electron beam, which

provide a clear structure vision by the microscope [12–14]. This is only possible due to the interaction between the electrons from SEM and the atoms in the sample. This constant interactions produce many signals that contain information about the surface topography and it own composition. An image is produce, then after a raster scan pattern by the electron beam pass through the surface and also the position of the focused beam combined with the intensity of the detected signal. Furthermore, there is a detector for the electrons from the excited atoms after been shooting with the beam from SEM [12–14]. The secondary electrons from the excited atoms detected by Everhart-Thornley detector and other related parameters like signal intensity among others are all related to the specimen topography. This technique allows a resolution in certain cases better than one nanometer [12–14]. Conventional SEM analysis are perform with the sample in high/low vacuum, also wet conditions are common with variable or environmental SEM pressure. Can be done with more several conditions such like cryogenic or elevated temperatures but required the combo with specialized instruments [12–14].

2.3 Electrochemical Techniques

Redox reactions based on the transfer of electrons between two species generate a potential differential. Each oxidation or reduction semi reaction have a typical potential differential associated.

The electrochemical sensors used in this study were screen printed carbon electrodes SPCE from *DropSens*, which have a three-electrode system. Made part of that three-electrode system are the working electrode, the counter electrode and the reference electrode. In the sensors used the working electrode is made by graphite (carbon), which is where the main experimental reaction occurs [15]. The counter electrode will always go against the working electrode to close the cycle, if the working electrode is taking an oxidation reaction in the counter electrode is a reduction reaction and vice-versa. The reference electrode is used a well-known electrical activity material such as silver [15].

2.3.1 Cyclic Voltammetry

When running a sensor in Cyclic Voltammetry (CV) it is possible to verify which species are under redox reactions. CV is run like the name subtends by cycling voltage between two values [16, 17]. In **(Figure 2.8)** the CV was run between 0 V and 1 V where the right arrow represent the flow of the charge and the left

arrow represents the discharge. Now, in case the sensor shows more activity when in contact with the study analyte, this means if the current raise in comparison to the value noted on the previous solution where it was missing, then it is concluded that the sensor detects this analyte in solution [16, 17]. Increments on its concentration usually increase current signal detected, which proves the sensing capacity of the modified sensor [16, 17].

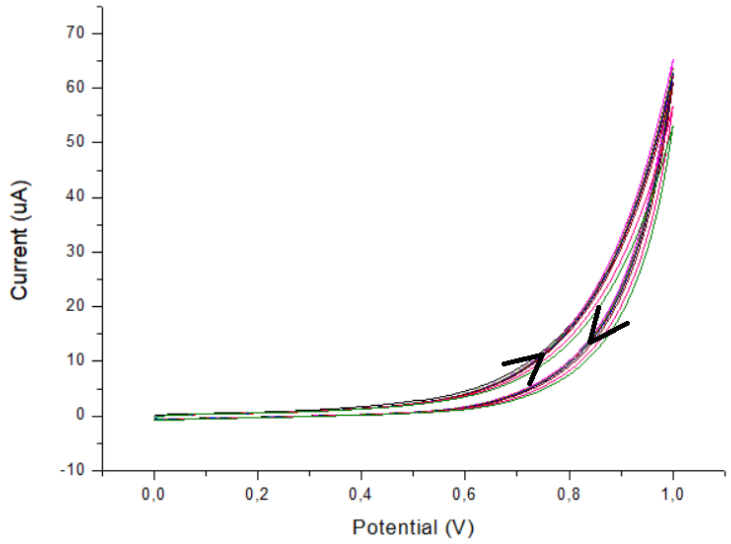

Figure 2.8: Screen-printed carbon bare electrode stabilization with schematic representation flow

After modify the working electrode the sensor is ready to run electrochemical trials, which is necessary to first stabilize it. This is possible by running this test to get the material compounds into a higher oxidation state, which allows the further oxidation of the analyte. Stabilized sensor will present overlapped CV curves, which mean both reactions are at equilibrium [16, 17]. CV with small doses of the analyte in the sensor medium allows to realize at which potential the active sites in the material at the working electrode produce a greater current spike. Is this potential that is further use in chronoamperommetry experiments [16, 17]. CV trials also permit the research group to compare different sensors results. Curves data analysis using adequate software allow to get the calibration curve. For this is calculate the increment between each analyte injection curve with the curve where the sensor was in an analyte free medium, by subtracting both current values at the optimal potential. For better data treatment is set up in the same plot different CV calibration curves from different sensors. This allows by simple observation which sensor presents better response to the analyte presence. A higher current increment usually set by the slope of the linear fitting curve

determines the best sensor.

2.3.2 Cyclic Voltammetry at Different Scan Rates

In order to check which step (kinetic reaction or diffusion) the catalytic process undergoes it is determine the release of the analyte in whatever nano-structure active sites that the material used to modify the sensor stands. Scan rate is change under constant analyte concentration. After data treatment of these results it is possible to get the calibration curve of this technique. Is calculated then the increment between each scan rate with the initial used, by subtracting both current values at the optimal potential set in the previous test. With that been said, in case of diffusion process controlled is observed at late scan rates the current trend to a constant number, becoming a hyperbolic kind of curve [16, 17]. That can be explained by the quicker the step scan runs in diffusion-controlled processes, the analyte does not have time to reach the place where redox reaction undergoes. Processes under diffusion control required a confirmation second plot where the potential is square rooted and the current is now linear dependent of potential currency. In counter way, processes that are kinetic controlled while the scan rate goes toward the highest values increment current values are still visible constant [16, 17], which leads to a linear calibration curve. The catalytic reaction as the first step it is always needed before diffusion, so it does not matter the value of scan rate use. The increment it still goes up linear due to rapid voltage submission [16, 17].

2.3.3 Amperommetry

Chronoamperommetry is perform in fix voltage, usually pre-defined as the voltage where the electro activity spikes (current peaked in CV test). This technique allows to get information on the current variation, such as if is proportional to fixed analyte injections increment in the tested solution [16, 17]. Getting consecutive "jumps" with the same variation values using same dosage from analyte solution predict an effective sensing response. Although chronoamperommetry trial is commonly interesting for the calculation of the electrode sensitivity (**(Equation 2.5)**, which is the main comparative parameter between sensors. Likewise the previous two techniques it is possible to get the calibration curve of this test. Is calculated the increment between each analyte injection with the zero analyte concentration values, by subtracting both current results [16, 17].

$$Sensitivity = \frac{Slope}{A} \tag{2.5}$$

$Slope$ = Slope of the fitting curve ($\mu A\ mM^{-1}$)
A = Superficial area of the working electrode (cm^2)

2.3.4 Selectivity and Repeatibility Tests

Despite the important of the previous referred parameter sensitivity, even if a sensor presents a huge result is not a viable one if fails this follow tests. By using the same technique, it is possible to perform two more experiments (selectivity and repeatibility). Selectivity tests intends to determine if the sensor also detects other analytes or just the one pretend. Several processes contain a ridiculous number of compounds undergoing the reaction medium [16, 17]. Using a sensor to detect a certain analyte that do not detect exclusively that same analyte can lead in misleading conclusions in some cases. Mostly if a known other analyte detected by the sensor is present in the solution medium. It is possible to check if the sensor only detects the pretend analyte and no other compound well known in the process undergoing, by using others analyte injections in the solution which the sensor is immerse. This is possible by verify if the current signal spikes when injected other analyte solution.

Repeatibility test just ensure the sensor properties remains the same over time. Consequent restarts on the chronoamperommetry trials allows to verify if the stabilized current value remains the same [16, 17] and take conclusions on sensor precision capacity. If is positive, the sensor is considered viable to use and misleading results are not confirmed by degradation. Parameters such as mean and standard deviation allow to better understand this crucial property referred above. The lower the standard deviation and consistency of the mean value imply a better sensor in term of repeatibility.

Chapter 3

State of Art

In this chapter is exposed fermentation and bioethanol processes related to the literature results in the last years. So, it is presented some basics about fermentation in section 3.1, also the explanation on each variables modify in order to achieve bioethanol fermentation to produce bioethanol and some literature reviewed techniques to monitoring this process. In section 3.2 is exposed literature reviewed in existing electrodes to the monitoring of glucose in solution. At the end in section 3.3 is a resume of the previous reviewed techniques before the start of the experimental part at chapter 4.

3.1 Fermentation

Fermentation is a well-known process, the fact it does not required oxygen make the metabolic path to anaerobic bacteria digestion [14]. Throw many steps is possible to convert the substrate in many diverse sub-products. The final low molecular weight organic products are mostly differed by the environment which fermentation undergoes. Changes in substrate, medium and microorganism can lead to different products. These products such as organic acids and alcohols (ethanol and others) can be guaranteed by set constant values/parameters associate with the previous referred properties [14]. Controlling these parameters such as temperature, pH, dissolved oxygen, liquid level and foam level towards the reaction time line is crucial and has been devoted by many to promise more efficient and yield results [18].

3.1.1 Bioethanol from Fermentation

With ethanol as a desire product, the substrate use are simple or complex sugars such as glucose [14]. Glucose is then converted in ethanol and carbon dioxide, which makes this process call ethanol fermentation. Many of the microorganisms that can go throw this process (ethanol fermentation) are counter intuitive inhibited by the ethanol itself, which acts as a yeast inhibitor [14]. So, in most of the industrial ethanol fermentation processes is used the yeast Saccharomyces cerevisiae because of its high tolerance [19]. In industrial mediums the maximum that ethanol concentration can be produce is 12 to 14% (v/v) of the medium [14].

3.1.2 Fermentation Sensors Application

Numerous techniques in the last decades appear as a response to this optimization control needs. Results using optical fiber sensor, in situ near-infrared spectroscopy (NIRS), biosensors and modified sensors (used in this thesis) were successfully reached. Without this techniques the monitoring of the parameters processes are highly time-consume and performed off-line in laboratories. Also require staff tasks, which are expensive and use non-"green" reagents that is well known to be against environmental surrounding [3, 18, 19].

Researchers developed a mathematical model which correlates the reflected intensity of light with diverse sugars concentration throw the fermentation process. The model was initially set and then, by collecting samples along the reaction timeline extrapolated to define constants. Optical fiber in both pure glucose solutions and complex sugarcane syrup samples allowed to reach ethanol medium concentration over fermentation process, as shown in **(Figure 3.1)**. The intensity reflected directly correlated with sugarcane concentrations along with first derivatives.

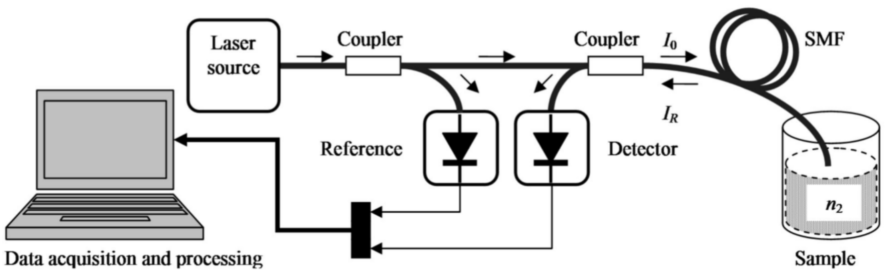

Figure 3.1: Configuration of the fiber sensor [3]

Despite automated, low-cost, real-time response and minimal invasive solution the results present in **(Figure 3.2)** were considered approximation of the

real values and not accurate [3].

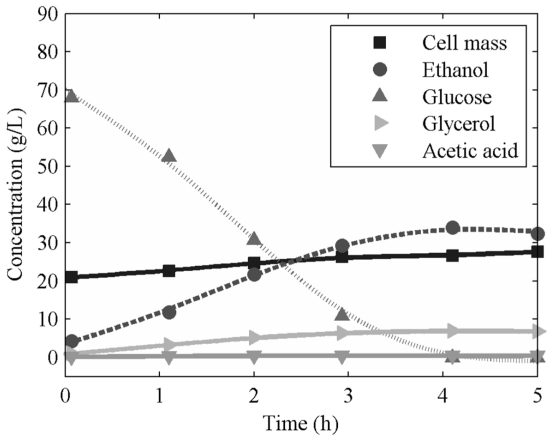

Figure 3.2: Laboratory analysis results for batch fermentation of glucose solution [3]

Such like the previously study, but in this case glucose and ethanol prediction was admitted as poorly precise data results. Using NIRS method along by taken several samples allowed to get calibration and validation data. This due to further characterization in high-performance liquid chromatography (HPLC) after centrifuge the collected sample in solid residue state. This two techniques can be scaled up to industrially processes and therefore optimize to better controlling results [19]. In this study it was set an apparatus like the scratch shown in **(Figure 3.3)**.

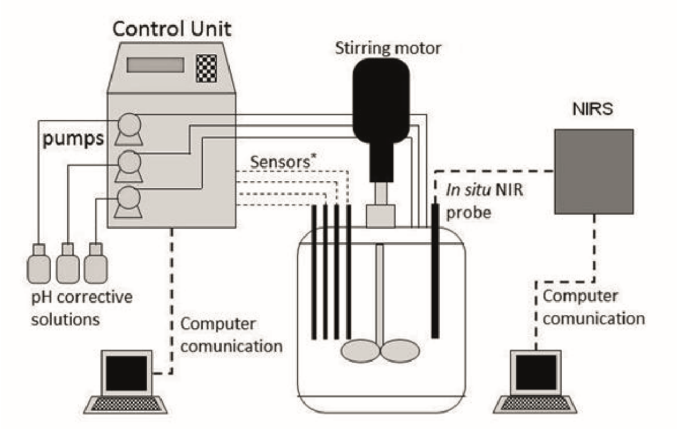

Figure 3.3: Schematic diagram of the experimental system. Sensors: pH sensor, dissolved oxygen sensor, level sensor and foam sensor [19]

In bioethanol fermentation processes all analyses required were time-consuming and were performed offline. The monitoring of glucose, ethanol, glycerine and biomass concentrations also required many laborious tasks. These methods use

reagents that can put our environment in constant dangerous and are quite expensive ones.

This previous two groups of investigations tried to avoid these bottlenecks using near-infrared spectroscopy (NIRS) and optical fiber probe to evaluate the real-time monitoring of crucial parameters in bioethanol fermentation. Possessing a wide data bank of multivariate analyses allowed spectra collected in real-time to be correlated with analyte concentrations obtained from reference methods, which led to the results in **(Figure 3.4)**. These groups obtained spectrum under 1 min which reduce a lot the time of data acquired. Although, the experiment was perform in laboratory made solutions with just a good approximation of the reality values and may bring some complications at industrial scale by using colorful mediums where is no viable the use of spectrometers.

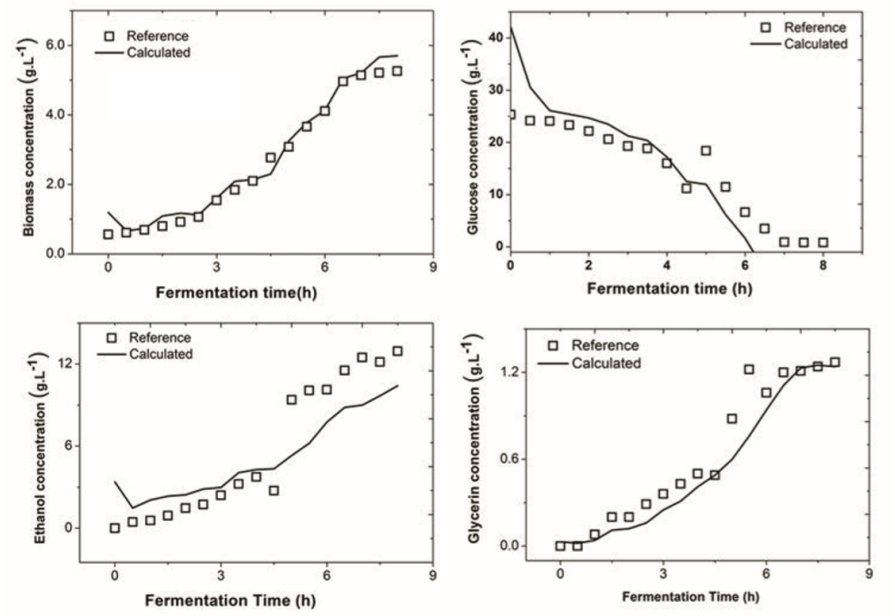

Figure 3.4: Kinetic curves obtained by the best NIRS model. The hollow symbols denote reference concentration values and the solid lines represent predicted concentration values [19]

The first bio-sensor was exposed in 1962 by fixing a layer of immobilized glucose oxidase (enzyme) membrane onto an electrode [18]. This sensor successfully detected dissolved oxygen concentration by transmitting a signal in form of volts due to the redox enzymatic reaction. This allowed the correlation to glucose concentration in solution [18]. Obviously, by the enzyme name the high selectivity is the major key for the effective sensing results. Since then many studies came using diverse biological constituents such as enzymes, antibodies and nucleic acids. Biosensors are inexpensive, easy preparation and shown to detect a

wide range of analyte concentration [14]. An ethanolic fermentation at laboratory scale was electrochemical monitored by constructed an enzymatic NADH electrode. Although was assumed by the research group a possible interference in the electrode sensing capacity due to the variable components present in reaction medium. The results shown in **(Table 3.1)** correlates the time in the fermentation process, viability of the yeast (which decreases while the ethanol concentration rises due to inhibition of the yeast activity) and ethanol/glucose concentrations.

Table 3.1: Time variation of the fermentation parameters [18]

Fermentation Time (h)	**Viability (%)**	**Glucose ($g \cdot 100\ mL^1$)**	**Ethanol ($mL \cdot 100\ mL^1$)**
0	81	12.20	0
3	68	11.99	1.32
5	65	11.90	2.08
7	63	11.20	2.81
24	59	9.25	5.54
26	46	7.87	5.70
30	45	7.02	6.25

Although the different application such as amino acid, sugar and alcohol detection result in the difficult of finding the most suitable bio element [18]. Researchers are still restricted to a limit number of modified biosensors, therefore further investigation and discovers need to be done so this promising technique can be more widely used.

3.2 Electrodes for Glucose Detection

The scope of this study is the glucose detection for bio-ethanol fermentation production processes. Glucose electrooxidation is a critical reaction that built the foundation for non-enzymatic glucose sensor development [16]. Thereby it was reviewed in literature many modified sensors. In order to modify tsensors was used diverse metal and metal-based materials, such as Co, Ag, Cu(II) complex, Iron, CuO, Ni, TiO_2 [15, 20, 21]. All this earth-abundant transition metals showed reasonable catalytic activities. From them there are still three preferable materials. Co, Cu and Ni showed great results due to their metallic, oxide and hydroxide forms catalytic capabilities [16]. As electrocatalysts for Co species, $Co(OH)_2$ and Co_3O_4 are the most common oxide forms used in sensing field. CuO, Cu_2O, NiO and $Ni(OH)_2$ likewise the Co species engaged as the electrocatalystst which many researchers use worldwide [16].

Despite the compounds previously described present a lower oxidation state, it is known the crucial role in glucose electrooxidation that the redox properties of the three species in higher oxidation states plays [16]. Alkaline mediums allows the electrooxidation of Co(II) previous form to Co(III) in form of CoOOH and Co(IV) form CoO_2 tipically essential compounds for glucose oxidation. Likewise, Cu(I) and Cu(II) to Cu(III) form CuOOH and also Ni(I) and Ni(II) to Ni(III) form NiOOH plays the key role in glucose electrooxidation for Cu and Ni species [16].

Different methods adopting differences in electronic and structural parameters have been impregnated over the years in sensor field community to achieve higher stability and efficient sensors. There are two variable ways. The first is through bimetallic compound formation, by consigning both advantageous properties in the same electrode. Many reports of this metals composite materials are present in literature such as Cu/Ti [22, 23] and also composites by assembly this transitions metals in graphene, carbon nanotubes [24, 25] introduced as a catalytic support for electrooxidation charge transfer between the material compound and the electrode itself. The second way which is a much more strategical one, by increase the number of reactions sites. Which means increase the surface area of the compound in the electrode, by leading to a much larger number of catalytic reactions. This engage the electrooxidation of the analyte and therefore yield a more efficient sensor [16]. Thin layers or porous structures are commonly the morphological structures desired by using techniques such as controlled deposition or directly formation in electrode surroundings [16].

In a really recent study from 2019, researchers successfully use glassy carbon electrode with three homogeneously dispersed transition metal ions. (Co(II), Cu(II) and Ni(II)) was injected in the alkaline electrolyte to enhance glucose sensing activity following **(Equation 3.1, 3.2 and 3.3)**.

$$Co + 2OH^- <=> Co(OH)_2 + 2e^- \tag{3.1}$$

$$Co(OH)_2 + OH^- <=> CoOOH + H_2O + e^- \tag{3.2}$$

$$CoOOH + glucose <=> Co(OH)_2 + glucolactone + e^- \tag{3.3}$$

Ni(II) and Cu(II) redox reactions are described elsewhere. As described in **(Chapter 2)** CV analysis provides enough information to set the current voltage where the material is more responsive activated. Thereby, in order to perform chronoamperommetry experiment with the set voltage and extract the sensitivity value from the calibration curve. After running cyclic voltammetric and

chronoamperometric electrochemical tests with different concentration of the dispersed transition metal ions in solution, the group was able to plot the data shown in **(Figure 3.5)**. This allowed them to find out the best compound perform with most sensitivity. The conclusion revealed to be the Co(II) with 1342 mA $M^{-}1$ cm $^{-}2$ the most capable of glucose detection followed by Cu(II) and at least Ni(II) with 579 and 38.9 mA M^{-1} cm $^{-}2$, respectively [16].

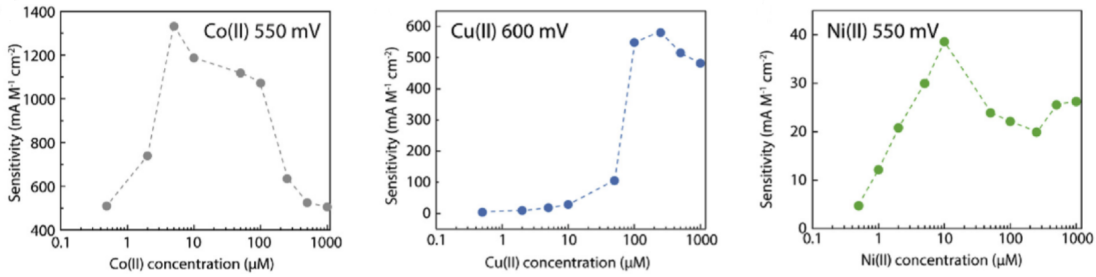

Figure 3.5: The sensitivity of glucose detection at a selected applied potential [16]

Despite the really good result with Co(II) dispersed in solution and the low laboral tasks perform for the preparation of the sensor for many reactions this process is not viable. The ion itself can act as an inhibitor since they used a bare carbon electrode with the ion dispersed in solution medium. A solution is modify electrodes with layers of compounds desire to home the catalytic electro-oxidation of glucose, which avoid this situation and proceed with a more sustainable solution.

An experiment using Ni in a carbon-silica matrix (N-CS) copulated with a more sophisticated process (formation of a metallic amorphous phase of the compound) showed a high sensitivity of 585 $\mu A\ mM^{-1}\ cm^{-2}$ in comparison to other literature results. Despite the complex preparation process in this study, the sensor was still prepare by simple deposition technique of dropping the solution in the carbon working electrode present in the screen printed electrodes [24]. In this case was necessary to activate the Ni so it is viable for catalyze the electrooxidation of glucose. Cycling the sensor in a 0.1 M KOH solution allowed the nickel itself to transited for an higher oxidation state by the following **(Equations 3.4 and 3.5)**

$$Ni + 2OH^{-} <=> Ni(OH)_2 + 2e^{-} \tag{3.4}$$

$$Ni(OH)_2 + OH^{-} <=> NiOOH + H_2O + e^{-} \tag{3.5}$$

After CV cycles in the KOH solution the Ni compounds from **(Equation 3.5)** allowed to proceed for CV test and determine the optimal potential response activity due to the reaction in **(Equation 3.6)** electro signal.

$$NiOOH + glucose <=> Ni(OH)_2 + glucolactone + e^- \tag{3.6}$$

Noticing a peak activity surrounding the 0.6 V of applied potential the group performed chronoamperommetric sensor test applying that same potential. This led by analytically data treatment get to the calibration curve present on **(Figure 3.6)** and consequently take the sensitivity result from the slope of the curve.

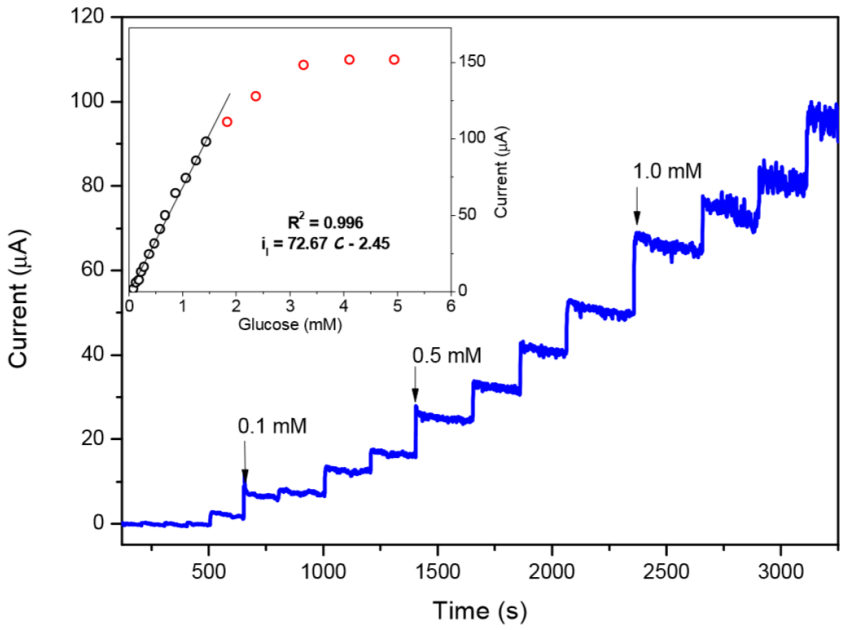

Figure 3.6: Chronoamperometry in 0.1 M KOH after successive additions of glucose at an optimal applied potential of 0.6 V [16]

A similar study from the previous one (same group) where Ni was impregnate in a carbon-matrix due to NiO reduction, but in this the sensor was put in medium with other compounds presents like pyrogallol-formaldehyde otherwise the silica in the above experiment. In this case different composites were study with different amounts of nickel, but the one that shown a better result was pyrogallol-formaldehyde loaded with Ni (PF/Ni30) (where the 30 stands for the percentage ratio between the reagents used pyrogallol-formaldehyde and nickel oxide) [17]. Due to the same based compound (niquel) the optimal applied potential remained the same at a value of 0.6 V. The chronoamperommetric test revealed in **(Figure 3.7)** a sensor sensitivity value of 670 $\mu A\ mM^{-1}\ cm^{-2}$ higher than the silica/niquel composite.

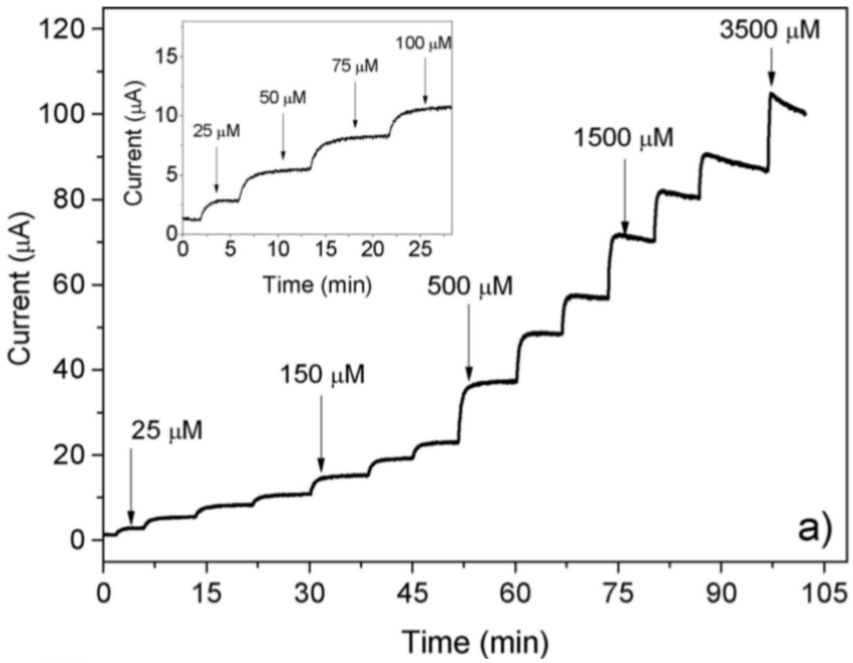

Figure 3.7: Chronoamperometric response of PF/Ni30 during different additions of glucose in 0.1 M KOH at an applied potential of 0.6 V [17]

Both experiments [17, 24] despite the good sensor response sensitivity resulted in a complex process of assemble the composite before electrode deposition. At industrial levels these difficult process can lead in a less yield process overall, which is resumed in a much larger financial input to begin with.

A much more simple preparation was successfully reached, by dispersing Ni nanoparticles in the porous surface of carbon so can after been enhanced the glucose electrooxidation. Likewise the simplicity of the process, the results after some electrochemical tests shown to be much less sensitivity than in the two previous and more complex sensor preparation studies [25]. In this particular case the group focus more on extract a huge advantageous from the material. They focused more on built a material with a wide surface area since it was only used nickel to get the final composite. Much likely the other two experiments the electrochemical tests shown in **(Figure 3.8)** were run in the same way. Although, the material output a sensitivity value of 146 $\mu A\ mM^{-1}\ cm^{-2}$, which is almost three times less the other two much more complex preparation processes.

The complexity of the sensor preparation at industrial scale can make a significant difference since the cost of tasks employed by laboral workers would be much superior than when it comes to a easy electrode assemble. The ultimate goal for glucose detection in bioethanol fermentation is a simple, inexpensive and sustainable sensor electrode that achieve high sensitivity in running tests, due to

is large scale size .

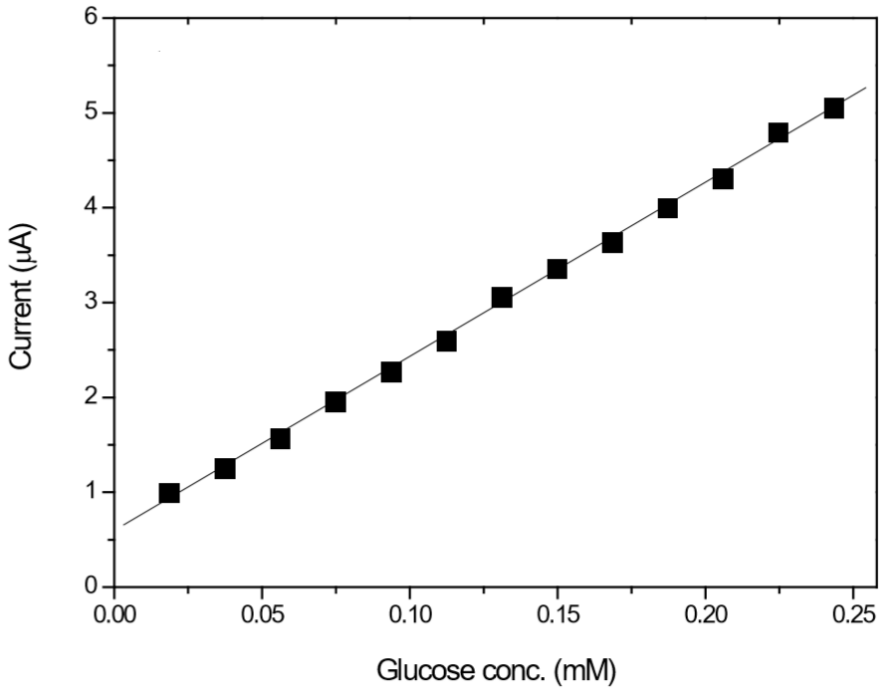

Figure 3.8: Amperometric calibration curve of the Ni-NC/SPCE electrode at the potential of 0.6 V [25]

In another study CuO nanostructures were grown on carbon working electrode. The group runned several electrochemical tests to optimized the deposition technique, which is the process to get the modified sensor. The aim of this study described here [26] was to compare the difference in sensor performs between in-situ growth of nanostructures and simple deposition techniques. Deposition technique is well described elsewhere in this document. Although in-situ growth requires a much more precise laboral control. The crystals of the compound growed directly on the electrode itself for preparation of the material to the electrochemical test that proceed. In-situ growth shows to be higher sensitivity with 1460 $\mu A\ mM^{-1}\ cm^{-2}$, selectivity and durability final sensor form than in the other methods [26]. Again this work [26] showed great results, but would still face some difficulties at industrial scale. Although in my opinion this sensor here in described is the best from the literature reviewed. It balances the complexity of the process with the results output, what makes it desire for practical uses.

Recently, a well developed and deeper study were perform by incorporate TiO_2 with CuO nanoparticles. This two compounds together were investigated due to photoelectrochemical well know properties shown by titanium kind of

materials. The researchers in this work conclude that TiO_2 inhibited the nucleation and growth of the copper oxide nanoparticles, which in comparison to pure modified CuO working electrodes raised the surface area of the sensor. Thereby a larger surface area provides more suitable conditions for glucose electro-oxidation.Consequently enhancing electrochemical results. Different Cu loading were prepared with the TiO_2 compound to carry out electrochemical sensing tests under dark, laboratory light and halogen illumination [22, 23].

3.2.1 Copper (I) Oxide as Electrode for glucose detection

Copper (I) oxide (Cu_2O) (a non-toxic molecule) come from its primary material copper itself, which is an abundant available element presents on nature [13]. It synthesizes is inexpensive which called researchers attention in using this compound throw several fields like photovoltaics, batteries, catalysis and gas/bio sensing activities [12]. Also called cuprous oxide is a metal semiconductor with a p-type valence band [13]. The conduction/valence band "jump" has a value of approximately 2 eV, which is consider low transition energy required and it is characterized as a direct bandgap [10, 27].

Nevertheless, there are several problems that limit the use of copper oxide in these applications. Such as fast capacity decreases and poor cycling stability, which are caused by the large-volume change and low conductivity during cycling [12].

Promising approaches on different (Cu_2O) structures synthesis like nanocubes have been over the last few years the strategy that researches are focusing on [12]. Cuprous oxide nanocubes fabrication process unfortunately is very difficult and expensive at industrially large-scale view [12].

The three following equations **(Equation 3.7, 3.8 and 3.9)** compile to the reaction that this all document is about. This three reactions built up the fundamentals for the electrode sensor work, which each one occurs in each electrochemical trial. The first two equation in a more early stabilization/activation stage and third equation in a more advanced stage where the glucose oxidation core reaction leads to detection by the sensor.

$$Cu_2O + 2OH^- => 2CuO + H_2O + 2e^- \tag{3.7}$$

$$CuO + OH^- => CuOOH + e^- \tag{3.8}$$

$$CuOOH + glucose + e^- => CuO + OH^- + gluconolactone \tag{3.9}$$

3.3 Conclusions

Fermentation processes occur with many redox reactions, which it led to the use of electrochemical analysis techniques as a toll for accurate characterization and control. Several studies have accomplished the track of the subtracts, such as glucose, fructose and sucrose in ethanol fermentation. Trying to discover materials with more selectivity, sustainability and non-expensive matters is the key to the future of industrial electrochemical sensing processes [16]. In **(Table 3.2)** are exposed the prime results from the literature reviewed in this chapter.

Table 3.2: State of art electrocatalysts for glucose detection results

Electrocatalyst	**Applied potential (V)**	**Sensitivity** ($\mu A\ mM^{-1}\ cm^{-2}$)	**Year**	**Reference**
Co(II)	0.55	1342	2019	[16]
Cu(II)	0.60	579	2019	[16]
Ni(II)	0.55	38.9	2019	[16]
N-CS	0.6	585	2018	[24]
PF/Ni30	0.6	670	2018	[17]
Ni-NC	0.55	146.4	2015	[25]
CuO	0.6	1460	2017	[26]

Chapter 4

Preparation and Characterization

This chapter presents the preparation and characterization of the samples used in the sensors did by the group. Section 4.1 explains how the material was synthesized by the group and further characterization in section 4.2. Section 4.3 explains how the sensor was modified.

4.1 Preparation of the Cu_2O

4.1.1 Preparation of the Samples

The synthesizing of cuprous oxide structured nanocubes (NC) were perform using wet precipitation technique. The process started by dissolving 0.85 g (weighted in SBS-LW-300A Steinberg) of $CuCl_2 2H_2O$ (Sigma-Aldrich) in 500 mL of distillate water under magnetic stirring (with 78-1 JSAT thermal plate) at constant 60°C. Next step was adding 50 mL of a 2 M NaOH solution from mixing 80 g of NaOH (Sigma-Aldrich) in 1 L of distillate water and stirred for another 30 min. Finally, 50 mL of a 0.6 M ascorbic acid solution by dissolving 106 g of ascorbic acid (Sigma-Aldrich) in 1 L of distillate water was insert. Red copper oxide precipitate was noted and after only 3 h of stirring at constant 60°C the formation of precipitate came to an end. This was then separated from the rest solution after several washes with distillate water and ethanol using centrifuge from (KREW Instruments). Also dried vacuum oven (Fistreem Vacuum Oven) were applied at 60°C for 12 h. This process here in described able to synthesize Cu_2O NC-10,

but another sample Cu_2O NC-9 were prepared. Instead of adding the 2 M NaOH solution at 60°C, this one was inserted at constant room temperature [12, 13].

4.2 Characterization

4.2.1 Morphological and Optical Analysis

Through the X-ray Diffraction (Europe 600 from GNR) (XRD) of powders **(Figure 4.1)**, the crystallographic structure and the purity of the samples Cu_2O NC-10 and Cu_2O NC-9 were investigated. The presence of impurities has been excluded and the reflection planes present at 29.7°, 36.6°, 42.5°, 52.5°, 61.6°, 73.7° and 77.5° refer to the planes according to **(Equations 2.1 and 2.2)** with Miller Indices (110), (111), (200), (211), (220), (311) and (222), respectively belonging to the cuprous oxide ((JCPDS 75-1531) [12, 13]. The more intense signal in NC-9 sample in comparison to NC-10 sample can be explained and it is further confirmed in SEM images by the smaller particle sizes, which means a higher specific area.

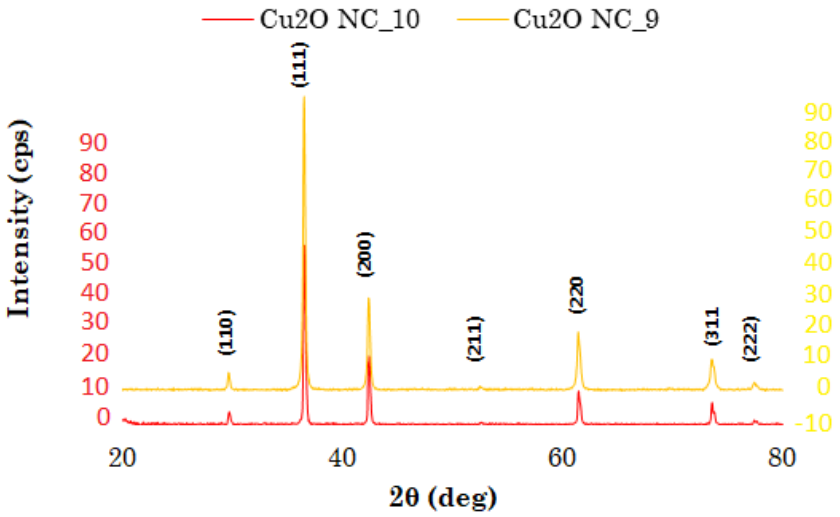

Figure 4.1: XRD spectra of samples Cu_2O NC-9 and NC-10

The optical properties were evaluated by UV-visible Diffuse Reflectance Spectroscopy shown in **(Figure 4.2)**, which made possible to measure the spectra in the range of 200-1200 nm.

Making resource of **(Equations 2.3 and 2.4)** was possible to compare the two catalysts in terms of band-gap through the Tauc plot measure in **(Figure 4.3)**,

The shift of the sample Cu_2O NC-9 ($E_g \approx 2,47$ eV) compared to Cu_2O NC-10 ($E_g \approx 2,03$ eV) is due to the smaller particle size causing a quantum confinement size effect, by considering that Cu_2O is a direct bandgap semiconductor and the

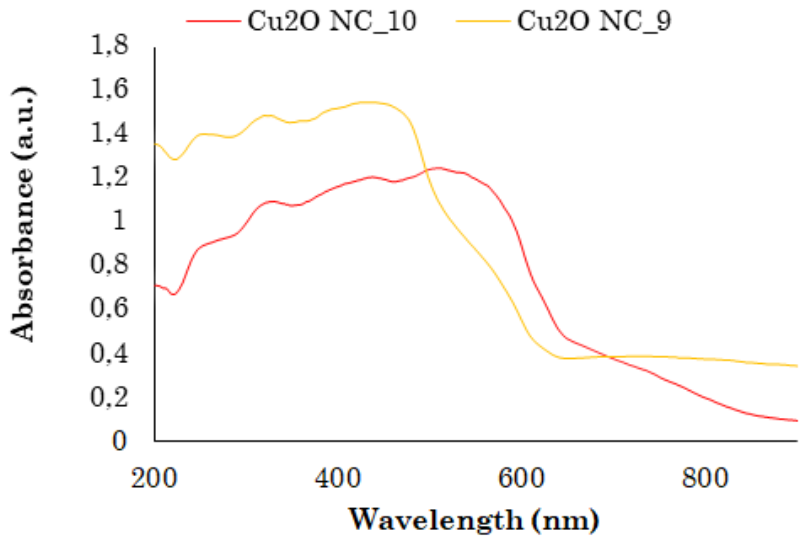

Figure 4.2: UV-visible Diffuse Reflectance Spectroscopy spectra of samples Cu_2O NC-9 and NC-10

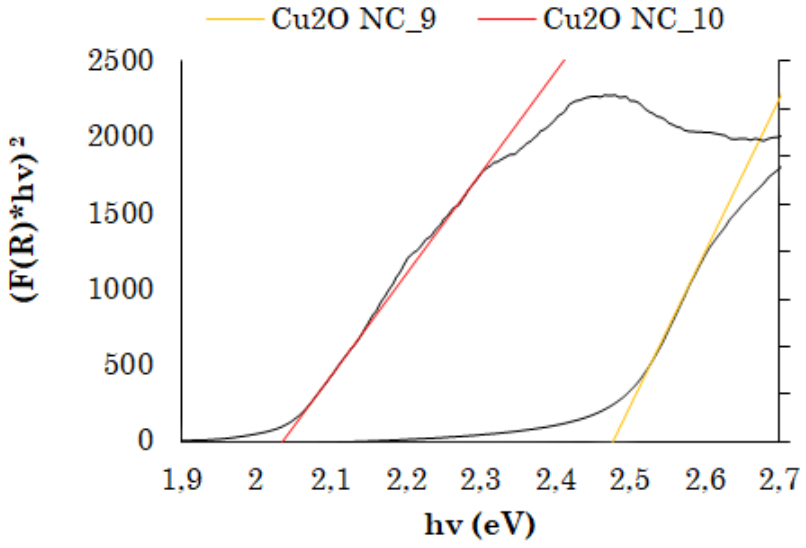

Figure 4.3: Tauc plot of samples Cu_2O NC-9 and NC-10

n exponent is assumed to be $\frac{1}{2}$ [12, 13]. As confirmed by UV-visible spectra (from SAFAS) and bandgap values calculated through the Tauc plot, the scanning electron microscope (SEM (NP6800 from Hitachi High-Technologies Europe)) analysis shows that Cu_2O NC-9 has a particle distribution ranging from 150 to 200 nm **(Figure 4.4a)** and for Cu_2O NC-10 from 200 to 900 nm **(Figure 4.4b)**.

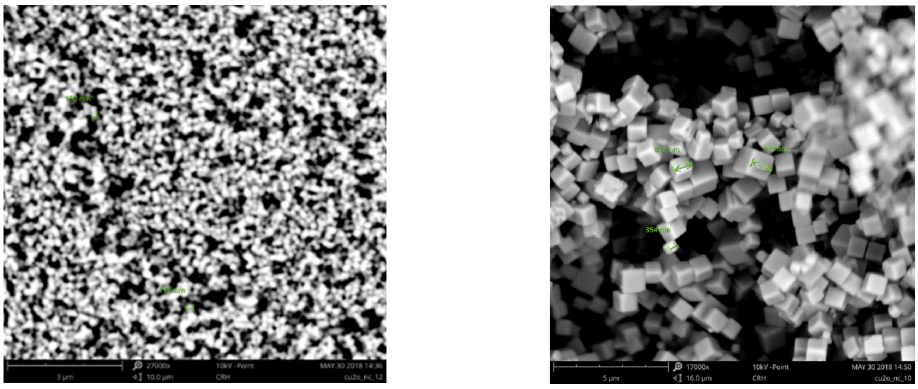

a) b)

Figure 4.4: SEM of Cu_2O samples: a) NC-9 scale: 1 cm = 2.0 µm; b) NC-10 scale: 1 cm = 3.3 µm

4.3 Preparation of the Sensor

4.3.1 Preparation of the Suspensions

After the preparation of both samples previously described, it was possible to prepare four suspensions. (NC-9, NC-10, P25 and HS-1) were required for the posterior deposition on the sensors. It was weighted 5 mg of each sample and added 100 µL of distillate water in to each Eppendorf. To mix and break some large grains present in the suspension, the two Eppendorf containing each sample suspension were putted in ultrasound equipment (TB-200 from AG SONIC) for 20 min.

4.3.2 Deposition Technique

The deposition performed on the working electrode was a process that required some patient and meticulous work. It was used for the deposition 5 µL of the previous suspension to prepare the sensor (one sensor for each sample suspension). Although the deposition was performed in two steps, which each one depositing 2.5 µL of the suspension. With the sensor on a thermal plate the first 2.5 µL were

applied using a micro pipette (MICROLIT). The thermal plate was set on and the sensor rested there for a couple of instants to dry the suspension by evaporation of the distillate water. That step allowed the sample particles settle in the working electrode nanopores. The sensor was then washed with distillate water to remove all the particles that did not settle on the pores and dried again at the thermal plate. This step was then repeated for the second deposition so after that the sensor shown in **(Figure 4.5)** was all prepared.

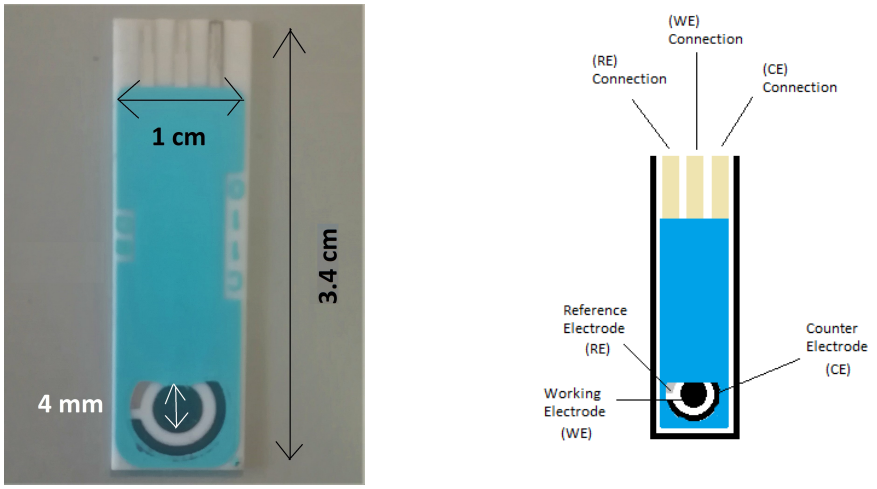

a) b)

Figure 4.5: Screen-printed modified carbon electrode representation: a) SPC Cu_2O electrode (NC9); b) Schematic representation of SPC modified electrode

4.3.3 Stabilization

This step is crucial in order to get the material in higher oxidation state ready to react to glucose. First, it was necessary to have a ground assay or zero one where a bare electrode was linked to the (DropSens) device, which led to the result present in **(Figure 4.6)**.

For that was required to submerse the electrodes in 5 mL of a potassium hydroxide (KOH) solution with 0,1 M concentration. With (Dropview) software the activity was track-able in order to start the stabilization of the sensor. After run in CV set up, the results shown in **(Figure 4.7)** defined the standard and it was possible to proceed for the modified SPCE, NC-9 and NC-10.

The two sensors now modified were then linked to the same apparatus one at the time. Using as method again cyclic voltammetry. It was set the tension induced to the electrodes with a step of 0.05 V/s starting at 0 V all the way to 1 V and as the name cyclic sub intends back to 0 V. The monitorization of the activity

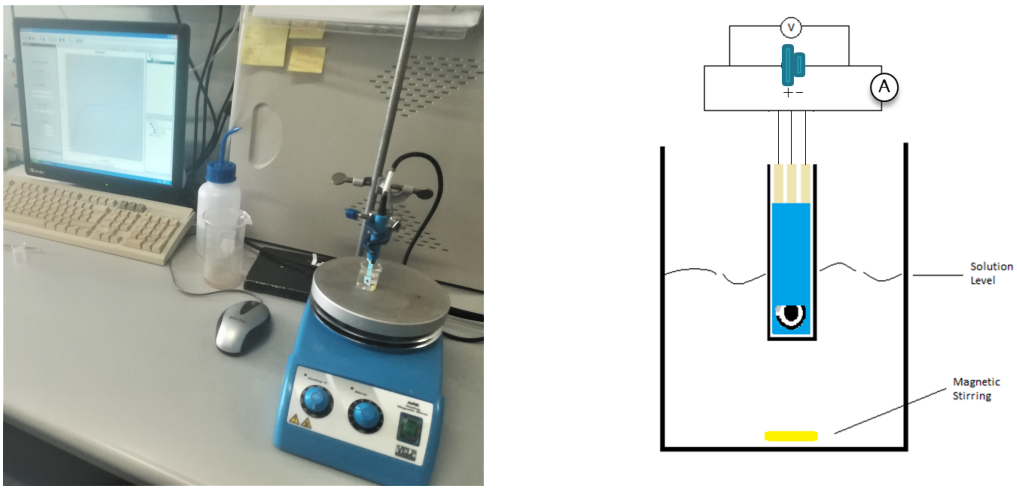

a) b)

Figure 4.6: Apparatus representation: a) Electrochemical Analysis Apparatus; b) Schematic representation of the apparatus

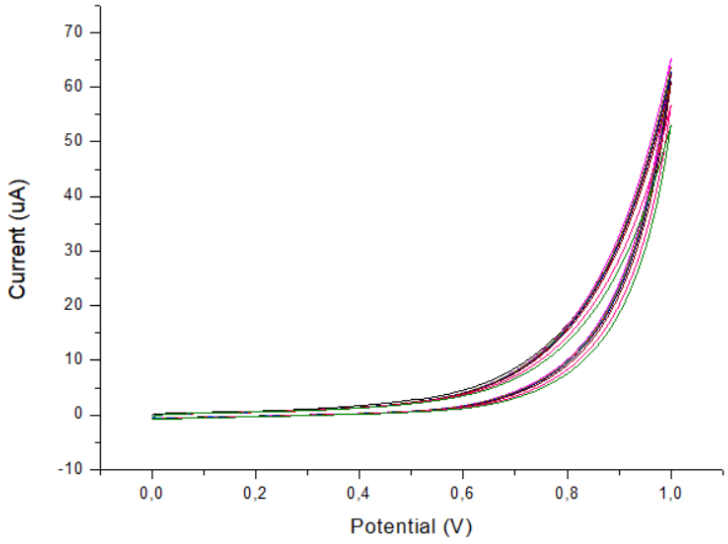

Figure 4.7: Screen-printed carbon bare electrode stabilization.

was possible by the current under potential curves shown at the software display shown in **(Figure 4.8) and (Figure 4.9)** .

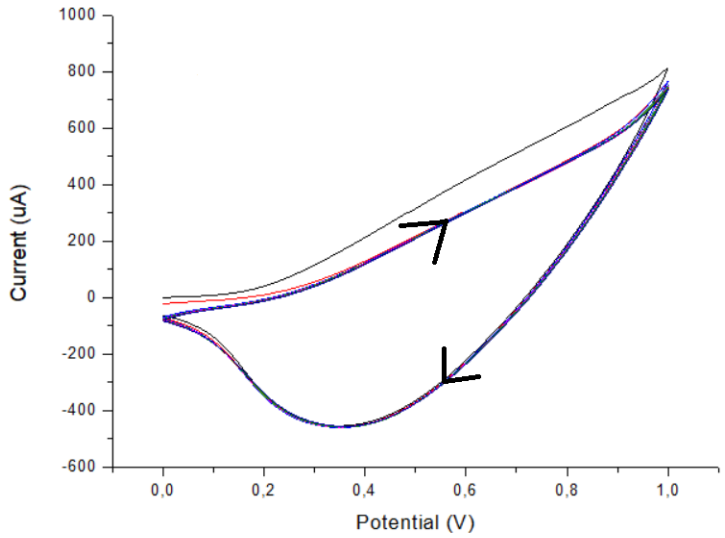

Figure 4.8: Screen-printed carbon NC-9 electrode stabilization.

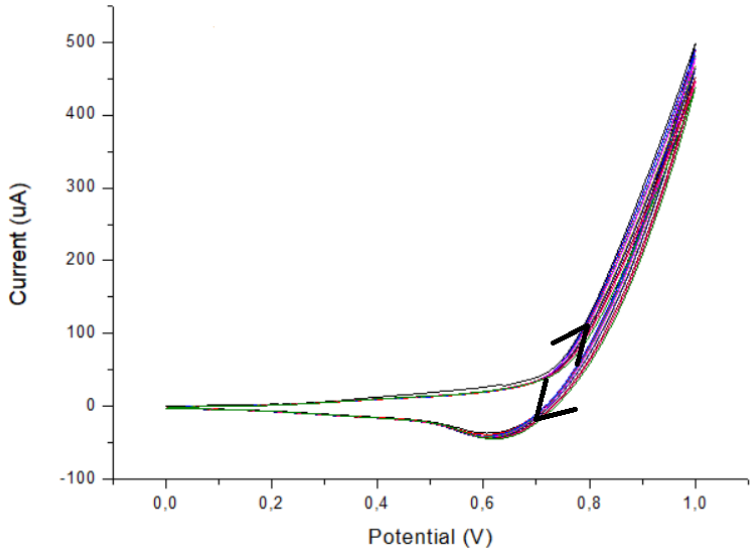

Figure 4.9: Screen-printed carbon NC-10 electrode stabilization.

This time the curves would have different signals from the previous bare one due to the oxidation of Cu_2O as mathematically exposed in the following **(Equations 4.1 and 4.2)**. The Cu(I) that stands at the electrode surface would now start to be oxidized and been convert to Cu(II) by the reaction in **(Equation 4.1)**. Consequently the Cu(II) was oxidized to a even higher oxidation state (CuOOH) Cu(III) by the reaction exposed in **(Equation 4.2)** [28, 29].

$$Cu_2O + 2OH^- => 2CuO + H_2O + 2e^- \tag{4.1}$$

$$CuO + OH^- => CuOOH + e^- \tag{4.2}$$

It was verified after some cycles that the curve would stay constant with the same values. The two reactions were then consider to be at equilibrium, which meant the sensor was then stabilized and ready for experimental usage.

Chapter 5

Results and discussion

This chapter presents all the electrochemical tests results such as CV, amperommetry, selectivity test and repeatibility test of the sensors in Section 5.1.

5.1 Electrochemical Analytical Results

5.1.1 Voltammetry

After stabilization procedure referred in **(Chapter 4)**, the experiment here in documented is a glucose sensitive test, which allowed the detection of glucose in solution. The potential applied in the sensor allows the oxidation of the copper oxide. This resulted in a certain current value. To run this experiment, it was performed 22 cycles by cycling applied potential between 0 V and 1 V (2 cycles of each concentration). In this 22 cycles is included the 1st two cycles with concentration of glucose 0 mM. In **(Chapter 2 and Chapter 3)** is shown that the oxidation transition of cooper oxide from Cu(I) for Cu(II) species and further to Cu(III) species required potentials between that applied range. Then with small injections directly on the solution sensor medium of a 50 mM mother solution (prepared dissolving 36 mg of glucose in 4 mL of the 0.1 M KOH solution), it was possible to run the glucose sensitivity test. This was only possible because the Cu(III) specie present in **(Equation 5.1)** reduced to able glucose electrooxidation, by giving CuO an Cu(II) specie and gluconolactone as products in the medium. The increment used was 1 mM of glucose. Begin with 0 mM all the way up to

10 mM as shown in **(Table 5.1)**. The volume injected is higher towards the final value of concentration due to the increase in the solution medium volume by the previous ones. Scan rate was kept constant at 0.05 V/s.

$$CuOOH + glucose + e^{-} => CuO + OH^{-} + gluconolactone \tag{5.1}$$

Table 5.1: Voltammetry glucose injection volume

Glucose concentration (mM)	**Volume injected (μL)**
0	0
1	102
2	106
3	111
4	115
5	121
6	126
7	132
8	138
9	145
10	152

The curves present in **(Figures 5.1 and 5.2)** shown a visible deviation for both samples which led to conclusion that the sensors using the two samples successfully detected glucose in solution. The data were treated by using an *Excel* like software (Origin), which allowed the assemblage of the values from CV in clear graphics. From the sensitivity trial curves were taken the 1^{st} of each concentration data to achieve a better resolution and results.

Then, it was calculated the intensity of current variation in both oxidation and reduction segment. This were taken in the range which performed a peaked greater variation. Although in further section the chronoamperommetry trials were perform with more than one pottential set (0.7 V), due to the non clear potential peak in **(Figures 5.1 and 5.2)**. The potential applied assumed that result in a wide current amplitude it was further confirm with chronoamperommetry, giving the value of 0.7 V. This value of 0.7 V is the potential where the Cu_2O is more electro-active for the reaction of glucose oxidation exposed in **(Equation 5.1)**. Subtraction of the current values intensity achieved in each concentration (different colors in **(Figures 5.1 and 5.2)**) represent different glucose concentration. With the value in concentration 0 mM was obtained for NC-9 and NC-10 sample oxidation calibration curves presented in **(Figure 5.3)** for the desired potential 0.7 V.

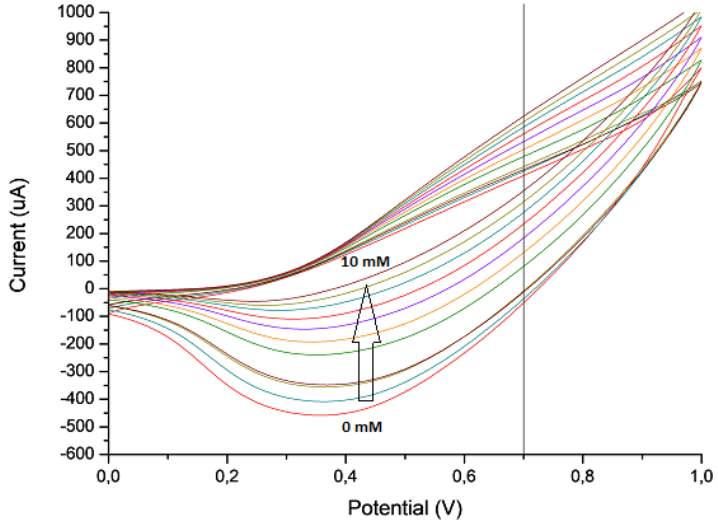

Figure 5.1: Cyclic voltammetry results of NC-9 performed at 0.1 M KOH

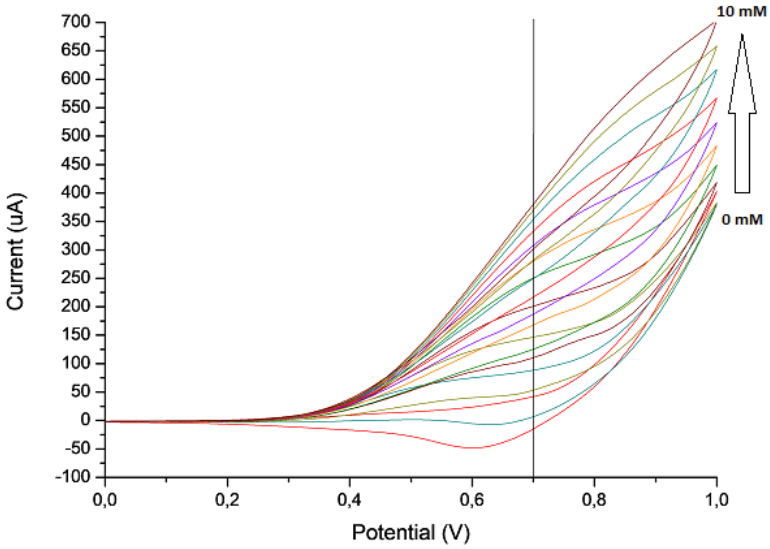

Figure 5.2: Cyclic voltammetry results of NC-10 performed at 0.1 M KOH

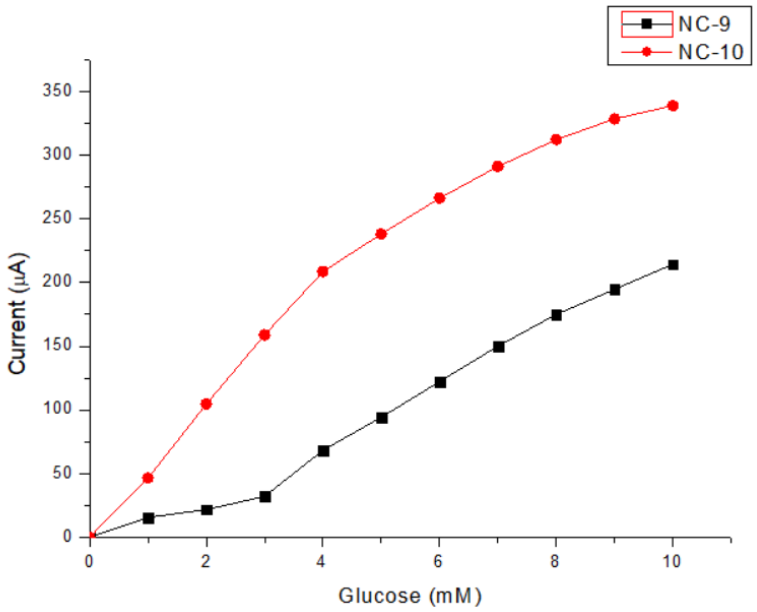

Figure 5.3: Cyclic voltammetry oxidation calibration curves for both samples NC performed at 0.1 M KOH

The results here in represented were no longer possible to repeat for sample NC-10. Also, further tests as CV at different scan rate were no longer viable. Possible cause is the leaching of the powder due to oversized particles relative to the carbon nanopores present in the sensor. In fact, the second trial of NC-10 sensor it was visible the leaching. This led to results similar to the bare electrode. For those reasons NC-9 became the main sensor study despite the better results taken from **(Figure 5.3)** by NC-10 sensor.

5.1.2 Voltammetry with Different Scan Rates

This technique allows the study of which mass transfer step (kinetic or diffusion) is the reaction under control. It was run CV at different scan rates (0.01 V/s to 0.1 V/s) along with constant glucose concentration (1 mM) in 5 mL of a KOH solution with 0.1 M concentration by injecting the desired volume of $102\ \mu L$ from **(Table 5.1)**. The data were treated similarly as for the CV analysis. The intensity of current variation in both oxidation and reduction segment where the current range performed a greater variation (in this case were 0.7 V for oxidation and a non-parallel line for reduction semi-curves as shown in **(Figure 5.4)**.

Then were subtracted the values of current intensity amplitude achieved in each concentration with the value at scan rate = 0.01 V/s (positive variation values for oxidation phase and negative variation values for reduction phase) to obtain oxidation/reduction calibration curves are presented in **(Figure 5.5)**.

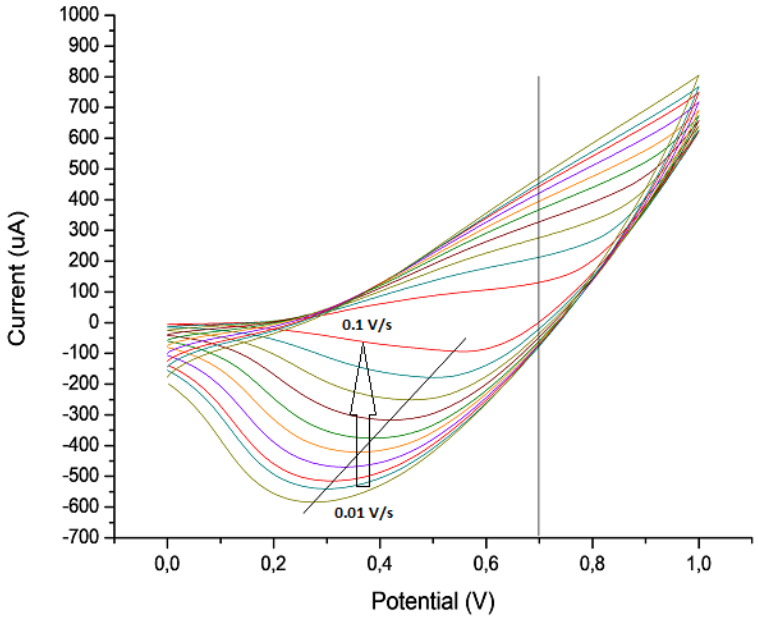

Figure 5.4: Cyclic voltammetry at different scan rate for sample NC-9 performed at 0.1 M KOH with 1 mM of glucose concentration

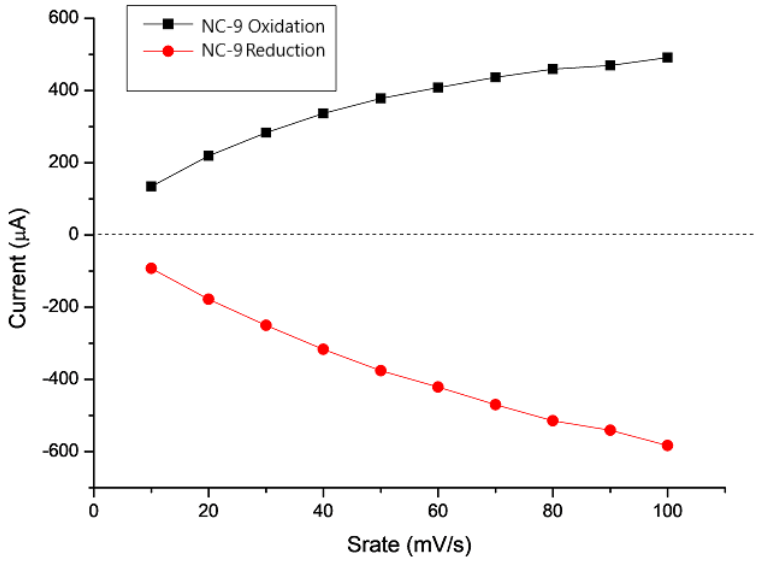

Figure 5.5: Calibration curve for NC-9 at different scan rates CV performed at 0.1 M KOH with 1 mM of glucose concentration

The non-linear calibration curve confirms that the reaction catalytic process is not under absorption control. Thereby, it was necessary to plot the $\sqrt{scanrate}$ *vs current* in **(Figure 5.6)** to confirm.

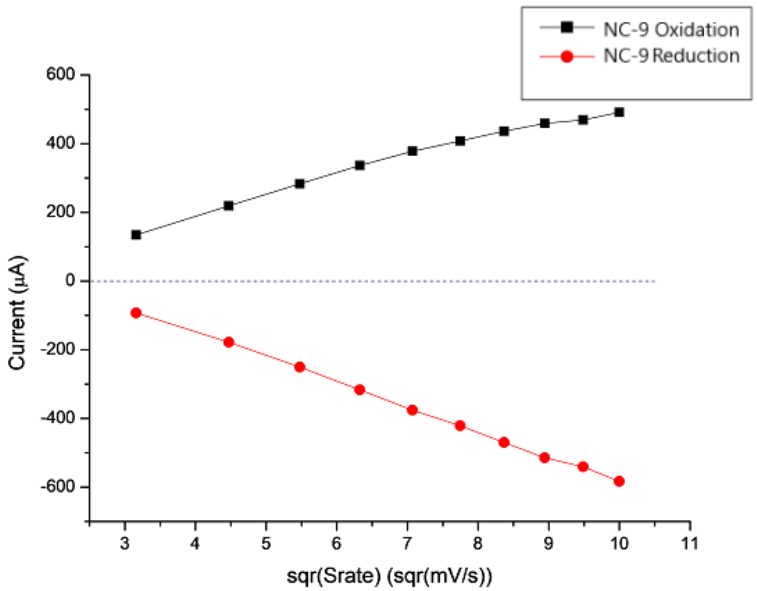

Figure 5.6: Cyclic voltammetry at different square roots scan rates results for NC-9 performed at 0.1 M KOH with 1 mM of glucose concentration

The process is controlled by diffusion (linear scan rate square root curve) as it is possible to visualize in **(Figure 5.6)**. That can be explained by the quicker the step scan runs in diffusion-controlled processes the glucose does not have time to reach the deeper copper oxide nanoporous. Is in this nanoporous where redox catalytic electrooxidation of glucose reaction undergoes.

5.1.3 Chronoamperommetry

The previous current peak visible in NC-9 sample CV curves (0.7 V) was set to perform chronoamperometry test in 5 mL of a KOH solution with 0.1 M concentration. Applying a (4x4) method present in **(Table 5.2)**, which means performing four sets of four equal volume injections from glucose mother solution. This method allowed to determine if the sensor response is proportional to the concentration of the analyte.

Each *"step"* that appeared on **(Figure 5.7a)** is associated with the sequentially injections from **(Table 5.2)**.The more volume of glucose present in solution, the bigger the spike in chronoamperommetric graph.

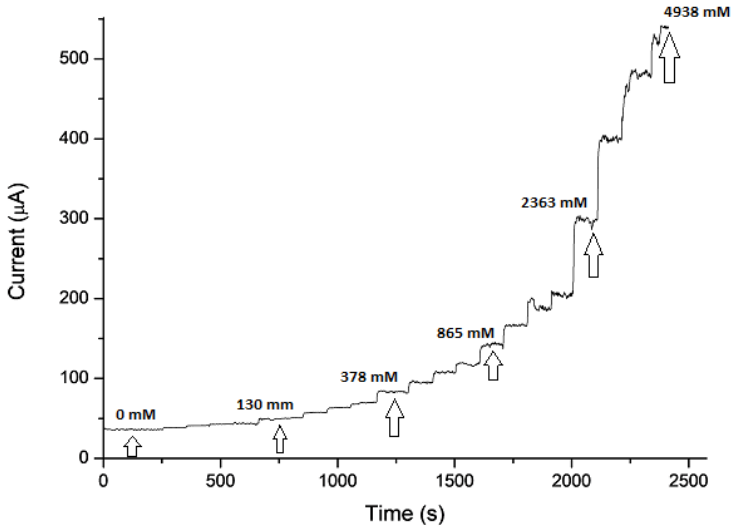

a)

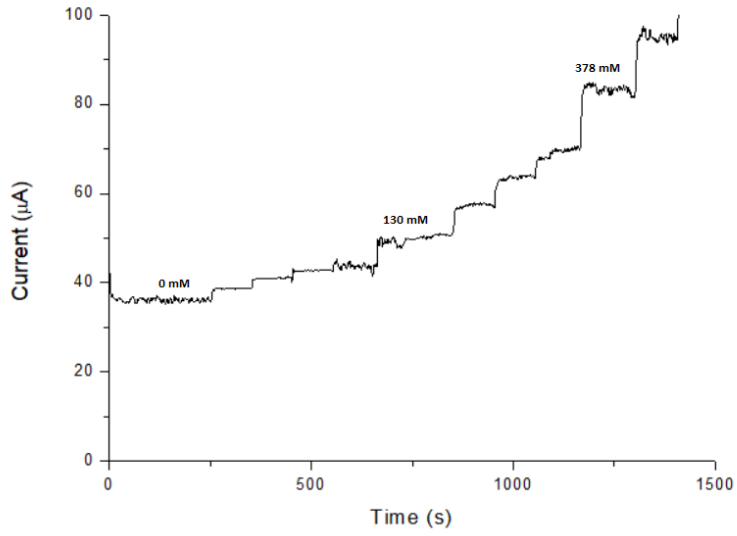

b)

Figure 5.7: Chronoamperommetry for sample NC-9: a) Chronoamperommetry for sample NC-9 at 0.7 V in 0.1 M KOH solution; b) Zoom-IN of the NC-9 chronoamperommetry at 0.7 V in 0.1 M KOH solution

Table 5.2: Amperommetry glucose injection volume

Glucose concentration (μM)	**Volume injected (μL)**
0	0
20	2
40	2
60	2
80	2
130	5
180	5
230	5
280	5
378	10
475	10
573	10
670	10
865	20
1057	20
1248	20
1437	20
2363	100
3253	100
4111	100
4938	100

Due to the previous referred in **(Section 5.1.1)**, it is necessary to confirms the strongest electro activity potential. Thereby it was perform four chronoamperommetric tests regard the NC-9 sensor. Each experiment with a different potential set described in **(Figure 5.8)**.

Similarly as for the CV analysis the data from **(Figure 5.8)** was treated. Subtraction of the current values achieved in every glucose concentration to the reference state (0 mM) to obtain calibration curves presented in **(Figure 5.9)**.

It is in fact confirm from **(Figure 5.9)** that at this potential of 0.7 V register the most catalytic glucose oxidation in Cu_2O activated sites. Chronoamperommetry is a test capable of measure the sensitivity of the sensor, which is the current measure for unit of glucose concentration and unit of superficial area. After isolation of the curve with best perform at 0.7 V potential, it was possible to extract the slope of the closest linear fitting represented in red at **(Figure 5.10)**.

Therefore was calculated the sensitivity parameter of the Cu_2O-SPCE modified sensor NC-9, by using the following **(Equation 5.2)** .

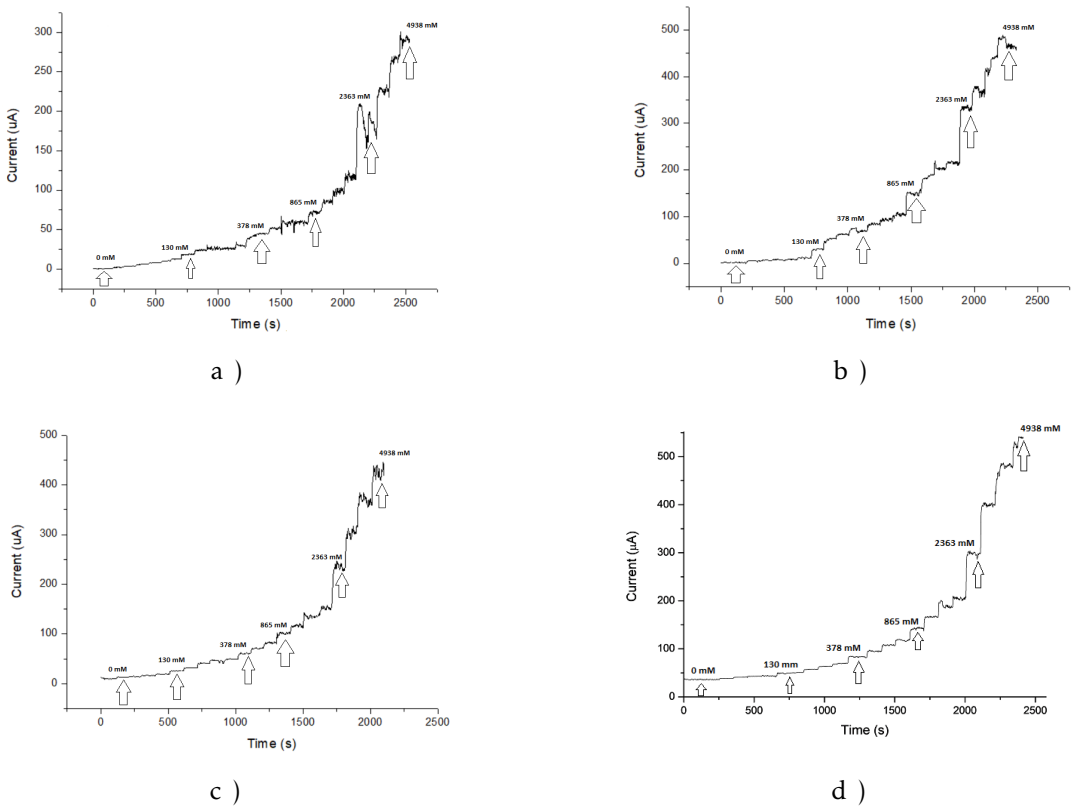

Figure 5.8: Chronoamperommetry for sample NC-9 at different potential applies in 0.1 M KOH solution: a) Chronoamperommetry for sample NC-9 at 0.5 V; b) Chronoamperommetry for sample NC-9 at 0.6 V; c) Chronoamperommetry for sample NC-9 at 0.65 V; d) Chronoamperommetry for sample NC-9 at 0.7 V

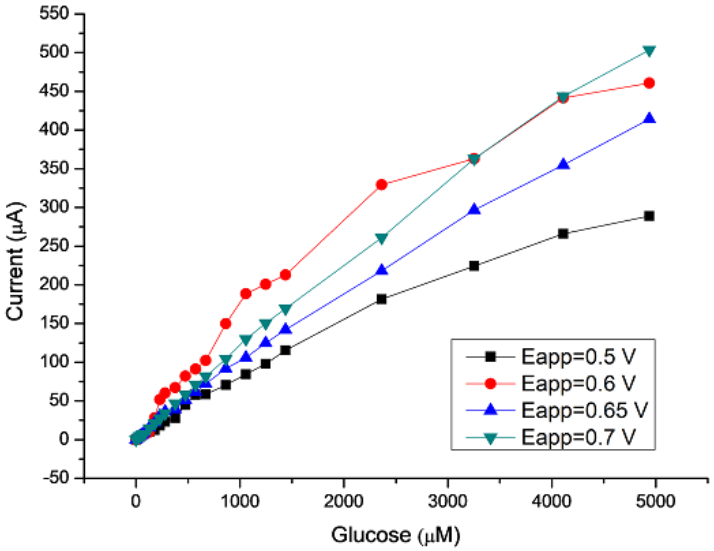

Figure 5.9: Chronoamperommetry calibration curve for sample NC-9 in 0.1 M KOH solution

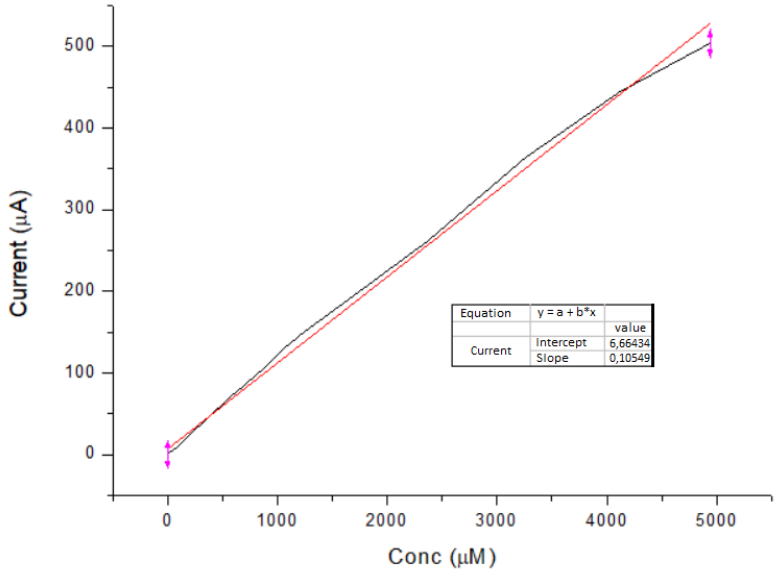

Figure 5.10: Chronoamperommetry calibration curve for sample NC-9 at 0.7 V with linear regression results

$$Sensitivity = \frac{Slope}{A} \tag{5.2}$$

$Slope$ = Slope of the fitting curve ($\mu A\ mM^{-1}$)

A = Superficial area of the working electrode (cm^2)

The SPCE (DropSens) working electrode have a 4 mm diameter. By simply applied the area of a circle ($\pi\ r^2$) is possible to get the result out of the previous equation. NC-9 presents a sensitivity of 840 $\mu A\ mM^{-1}\ cm^{-2}$. This value showed up a really competitive result in comparison to literature reviewed as present in (**Table 5.3**)

Table 5.3: Comparison of Cu(I)-ion catalyst with other state of art electrocatalysts for glucose detection

Electrocatalyst	**Applied potential (V)**	**Sensitivity ($\mu A\ mM^{-1}\ cm^{-2}$)**	**Year**	**Reference**
Co(II)	0.55	1342	2019	[16]
Cu(II)	0.60	579	2019	[16]
Ni(II)	0.55	38.9	2019	[16]
N-CS	0.6	585	2018	[24]
PF/Ni30	0.6	670	2018	[17]
Ni-NC	0.55	146.4	2015	[25]
CuO	0.6	1460	2017	[26]
Cu_2O	0.70	840	2019	This work

Despite the exclusion of NC-10 as a viable sensor because of the leaching matter referred above, chronoamperommetric tests were perform in order to confirm the situation of leaching. In (**Figure 5.11**) and (**Figure 5.12**) is quite noticeable the huge drop in current registered in comparison to CV results and even to NC-9 chronoamperommetric data.

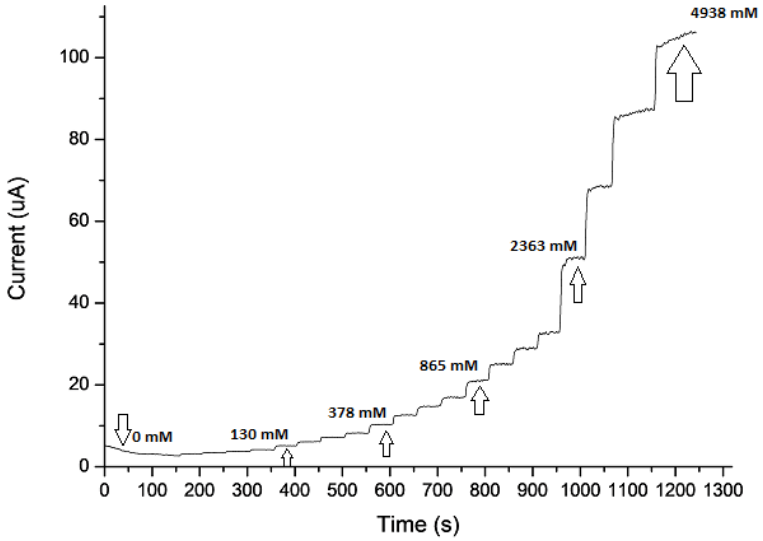

Figure 5.11: Chronoamperommetry for sample NC-10 at 0.7 V in 0.1 M KOH solution

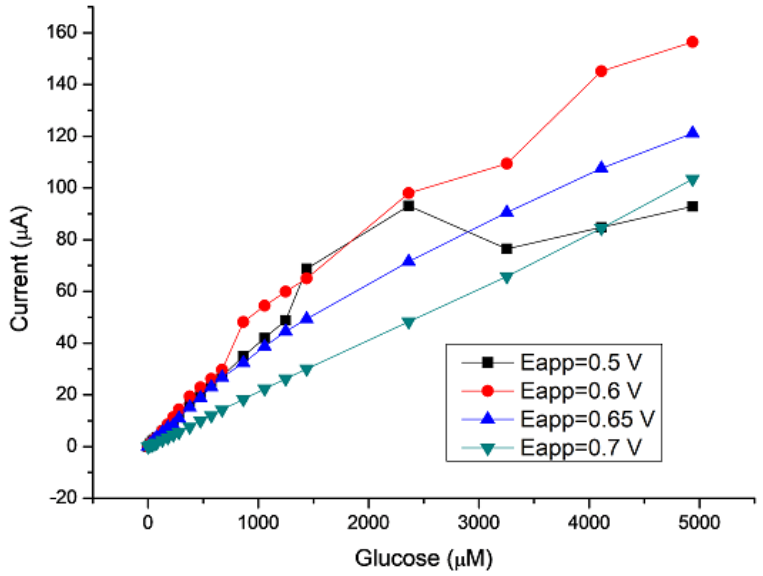

Figure 5.12: Chronoamperommetry calibration curve for sample NC-10 in 0.1 M KOH solution

NC-10 otherwise a great sensor by the results in (**Section 5.1.1**) was now consider unenviable and with worst results. In an electrochemical point of view it is considered worst than NC-9. NC-10 in CV trials appeared to ascend as the top sensor. Although is lixing problems were stronger than is sensitivity results. A possible solution to this problem is to find a glue type material that would give NC-10 a stick property to the electrode. Materials such as naflon are currently used in this situation where the compound is attached to the working electrode.

5.1.4 Selectivity Test

Another amperommetry technique was used, this time in order to test the sensor selectivity through injections of different analytes. The majority of them sugars, which the mother solutions preparation is present in (**Table 5.4**).

Table 5.4: Preparation of analytes mother-solution

Analyte	Mass of analyte dissolved (mg)	Volume of KOH 0.1 M solution (mL)
Glucose	36	4
Fructose	18	5
Sucrose	34	5
Marmose	18	5
Uric Acid	4	5
Dopamine	5	5
Ascorbic Acid	4	5

Different analytes solutions were used in a volume from mother solutions exposed at (**Table 5.5**). In order to perform the selectivity test was set in 5 mL of a KOH solution with 0.1 M concentration the senor. Was then compared the current response to the glucose injections. These ones were performed first and in last of the running experiment.

Table 5.5: Selectivity test analytes injection volume

Analyte	Volume injected (μL)	Mother solution concentration (mM)
Glucose	100	50
Fructose	20	20
Sucrose	20	20
Marmose	20	20
Uric Acid	100	5
Dopamine	100	5
Ascorbic Acid	100	5

As observe in **(Figure 5.13)** the sensor was effectually design to detect glucose in solution without influence of any other analyte like fructose, sucrose and marmose undergoing in reaction. Likewise, a small injection of ethanol before the last glucose injection did not spike any electrochemical reaction.

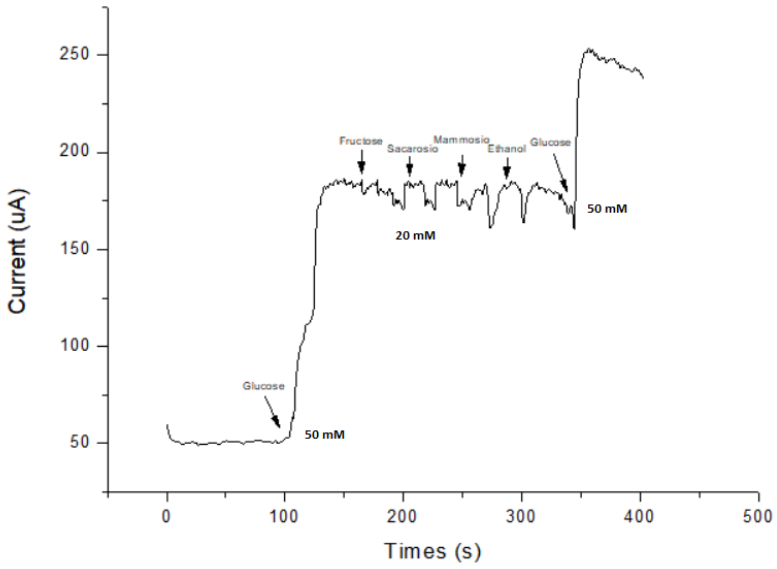

Figure 5.13: Selectivity results for NC-9 in 0.1 M KOH solution

The sensor NC-10 results in **(Figure 5.14)** were also take in a count at this test. Although resulted again in weak current responses due to previous justifications.

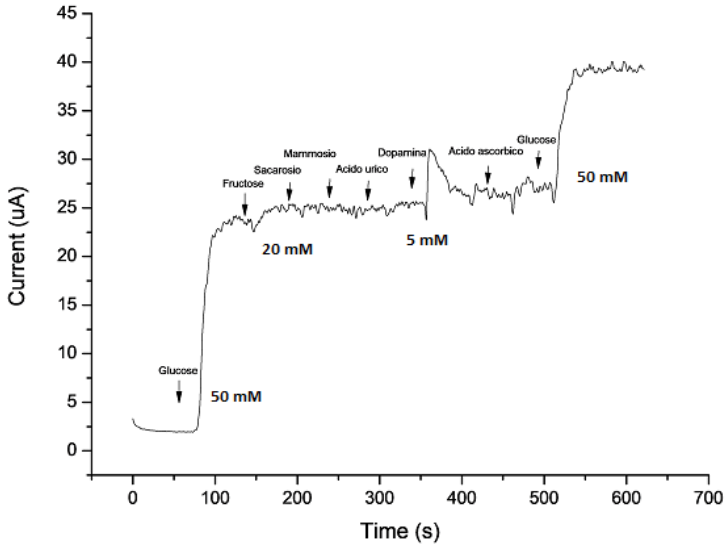

Figure 5.14: Selectivity results for NC-10 in 0.1 M KOH solution

Observation of both graphics at **(Figure 5.13)** and **(Figure 5.14)** it is noticeable the different analytes used, this is because NC-9 was the sensor "chosen"to

take for possible bioethanol fermentation process control. Therefore, NC-9 sensor did required running selectivity under conditions similar to the process called elsewhere. Analytes such as sugars (substrates present along the all process) and ethanol the desired by-product were tested.

5.1.5 Repeatability Test

Repeatability test was perform to ensure if the sensor properties remained the same with time. Consequent restarts on the amperommetry technique with 0 mM glucose concentration allowed to verify if the stabilized current value remained the same. Shown in **(Figure 5.15)** NC-9 performed repeatibility tendency current values. NC-9 presented coherent values along the three amperommetry tests: chronoamperommetry, selectivity and repeatibility.

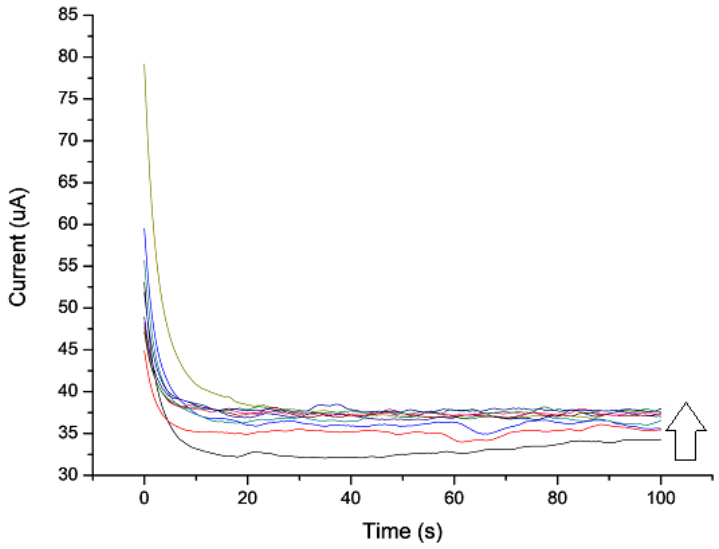

Figure 5.15: Repeatibility results for sample NC-9 in 0.1 M KOH solution

This test was the final electrochemical trial performed for each sensor. Here in shown in **(Figure 5.16)**, the NC-10 sensor was nearly full depleted. This means, the material once deposited and aggregated to the working electrode was now almost totally lixing and was not present at the electrode itself anymore. The very low current values observed are the result of it, which confirms the inability of use NC-10 in future work or at least how its stands.

The previous data were treated in order to verify mean and standard deviation of the repeatibility test. This analysis is presented in **(Figure 5.17)**. Both standard deviation values showed up great results. The lowish proportion of *mean vs standard deviation* implies a great repeatibility capacity for each sensor.

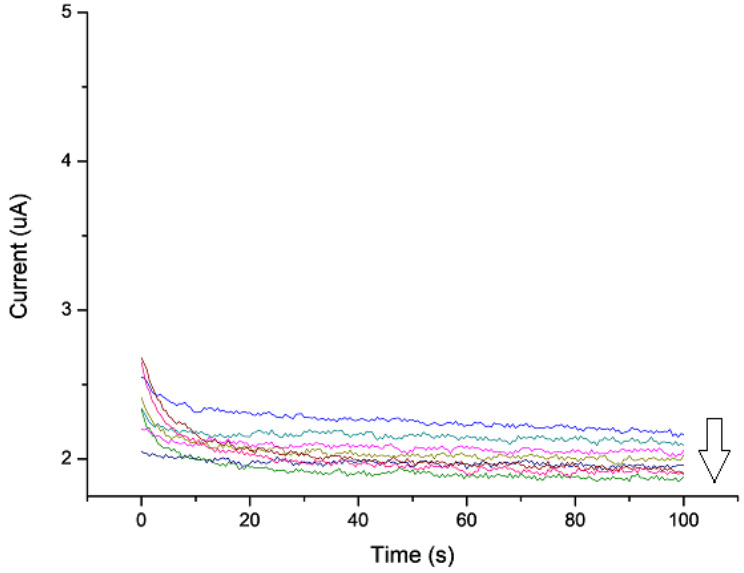

Figure 5.16: Repeatibility results for sample NC-10 in 0.1 M KOH solution

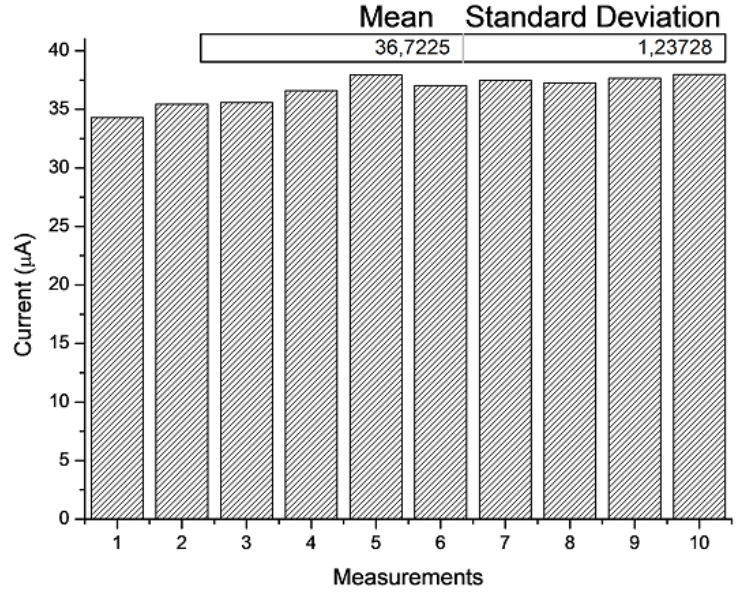

Figure 5.17: NC-9 repeatibility test mean and standard deviation in 0.1 M KOH solution

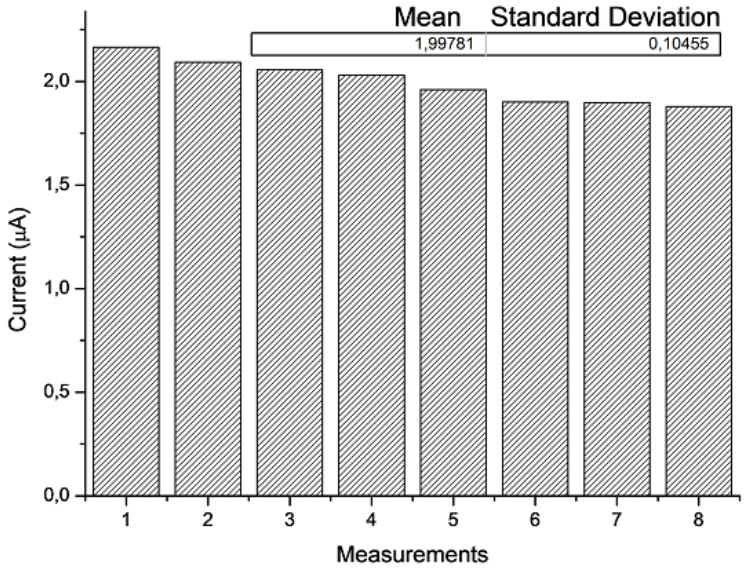

Figure 5.18: NC-10 repeatibility test mean and standard deviation in 0.1 M KOH solution

5.1.6 P25 and HS-1 Sensors

Another two sensors were prepared P25 and HS-1, which is a mix between copper oxide and titanium oxide and another copper oxide based sensor, respectively. Unfortunately this two were only available in the final powder form and was not possible to characterize them. Preparation of this both samples were not knew too. That is why the results of electrochemical trials for both sensors were kept in **(Appendix A)**. Despite P25 did not perform much different than sensor NC-10 in concern of the lixing affect. HS-1 shown as well nice performance on the experiments. Although is kept in mind that the result did not beat NC-9 sensor performance.

Chapter 6

Conclusion and Future Work

Cu_2O cuprous oxide was widely studied due to its amazing electrode properties. NC-9 and NC-10 structured crystalline nanocubes were deeply worked on. Electrochemical tests were run in all four sensors. The structured nanocubes previously referred NC-9 and NC-10 present sizes of 150-200 nm and 200-900 nm, respectively. The size differences is the main justification of the following NC-10 results conclusions.

Comparing the NC-9 sensor with the Zheng et al [16] first three results is observed that Co(II) transition metal dispersed in solution acquired a better sensitivity of 1342 $\mu A\ mM^{-1}\ cm^{-2}$. Although keep in mind that this technique is a little odd and invasive in comparison with a simple electrode. By allow different compounds in contact with the reaction medium can led to a disturbing action, which influence the final yield of the process.

The Niquel composite prepared by Zahmouli et al [24] referred afterwards by impregnation of Ni in carbon-silica matrix, despite the simple sensor preparation. Using one of the simplest technique (deposition) the Ni activation and matrix procedure was still consider a difficult methodical approach for the result output. In other words the sensitivity result from this work was 585 $\mu A\ mM^{-1}\ cm^{-2}$ but not worth the task in comparison to NC-9 sensor.

The next study from Marini et al [17] similar to the previous one result in the same situation, where the complexity of the procedure/laboral task were disproportional to the final sensitivity result of 670 $\mu A\ mM^{-1}\ cm^{-2}$. Keep in mind that this conclusions are always against NC-9 as a reference model. The

composite used (pyrogallol-formaldehyde) with Ni in a carbon matrix relies with a much more aware problem due to the difference in using PF instead of silica.

The last Ni article exposed by Mansour et al [25] against this last two allowed an easier preparation by simple use a niquel based composite with carbon, which resulted in a weaker value of 146.4 $\mu A\ mM^{-1}\ cm^{-2}$. Neither Ni sensor above revealed to beat NC-9 in sensitivity value. NC-9 is in fact easiest to assemble as the preparation of this Ni-C based composite using the same deposition technique.

CuO revealed to be the best sensor reviewed by Leonardi et al [26] with a sensitivity of 1460 $\mu A\ mM^{-1}\ cm^{-2}$. This sensitivity value much higher in comparison to the others and even to NC-9 sample of 840 $\mu A\ mM^{-1}\ cm^{-2}$, put this electrode in an elevated stance. Only the peculiar preparation by in-situ-growth method can subtend a more delicate technique. The real question is at industrial levels which one would be worth it, which basically regard a better yield process. CuO in-situ-growth or NC-9? The more than 600 $\mu A\ mM^{-1}\ cm^{-2}$ displacement between this two sensors are worth the minute technique? I believe this question would be easily answer by scaling both project up to the industrial scale. Nevertheless, NC-9 sensor it was easily managed and prepared, which resulted in a great competitive value with possible further updates.

NC-10 the other cuprous oxide modified sensor based electrode showed up great results in CV first trials. Although in the left electrochemical experiments was consider unenviable due to lixing problems. A possible solution in future work is to find a glue type material that bond with NC-10 compound and possible get more adherent to the working electrode. Materials such as naflon are currently used in this cases.

The other two sensors prepared P25 and HS-1, a mix between copper oxide and titanium oxide and another copper oxide based sensor were successfully run in electrochemical tests, respectively. Unfortunately this two were already prepared when reach the group in the final powder form and was not possible to characterize them. Preparation of this both samples were not knew too. That is why the results of electrochemical trials for both sensors were kept in **(Appendix A)**. Despite P25 did not perform much different than sensor NC-10 in concern of the lixing affect, HS-1 shown as well nice performance on the experiments. Although is keep in mind that the result did not beat NC-9 sensor performance.

Certainly the future investment should be on the NC-9 and NC-10 sensors, by solving NC-10 lixing problem can lead to a promise sensor.

Bibliography

[1] M. Vohra, J. Manwar, R. Manmode, S. Padgilwar, and S. Patil. "Bioethanol production: Feedstock and current technologies." In: *Journal of Environmental Chemical Engineering* 2.1 (Mar. 2014), pp. 573–584. DOI: 10.1016/j.jece.2013.10.013. URL: https://doi.org/10.1016/j.jece.2013.10.013.

[2] H. Zabed, J. Sahu, A. Boyce, and G. Faruq. "Fuel ethanol production from lignocellulosic biomass: An overview on feedstocks and technological approaches." In: *Renewable and Sustainable Energy Reviews* 66 (Dec. 2016), pp. 751–774. DOI: 10.1016/j.rser.2016.08.038. URL: https://doi.org/10.1016/j.rser.2016.08.038.

[3] E. Fujiwara, E. Ono, C. K. Yamakawa, J. L. Ienczak, C. E. V. Rossell, and C. K. Suzuki. "Real-time monitoring of fermentation process applied to sugarcane bioethanol production." In: *OFS2012 22nd International Conference on Optical Fiber Sensors*. Ed. by Y. Liao, W. Jin, D. D. Sampson, R. Yamauchi, Y. Chung, K. Nakamura, and Y. Rao. SPIE, Oct. 2012. DOI: 10.1117/12.970511. URL: https://doi.org/10.1117/12.970511.

[4] R. F. Association. *Global ethanol production*. 2018. URL: https://afdc.energy.gov/files/u/data/data_source/10331/10331_world_ethanol_production.xlsx.

[5] C. E. Wyman. "Ethanol Fuel." In: *Encyclopedia of Energy*. Elsevier, 2004, pp. 541–555. DOI: 10.1016/b0-12-176480-x/00518-0. URL: https://doi.org/10.1016/b0-12-176480-x/00518-0.

[6] M. D. D. Oliveira. "Sugarcane and Ethanol Production and Carbon Dioxide Balances." In: *Biofuels, Solar and Wind as Renewable Energy Systems*. Springer Netherlands, pp. 215–230. DOI: 10.1007/978-1-4020-8654-0_9. URL: https://doi.org/10.1007/978-1-4020-8654-0_9.

[7] Boden, T.A., G. Marland, and R. Andres. *Global, Regional, and National Fossil-Fuel CO2 Emissions*. 2017. URL: https://cdiac.ess-dive.lbl.gov/trends/emis/tre_glob_2014.html.

[8] R. F. Pierret. *Semiconductor Fundamentals: Volume I (2nd Edition)*. Pearson, 1988. ISBN: 0201122952. URL: https://www.xarg.org/ref/a/0201122952/.

[9] S. H. Simon. *The Oxford Solid State Basics*. Oxford University Press, 2013. ISBN: 0199680760. URL: https://www.xarg.org/ref/a/0199680760/.

[10] M. Yin, C.-K. Wu, Y. Lou, C. Burda, J. T. Koberstein, Y. Zhu, and S. O'Brien. "Copper Oxide Nanocrystals." In: *Journal of the American Chemical Society* 127.26 (July 2005), pp. 9506–9511. DOI: 10.1021/ja050006u. URL: https://doi.org/10.1021/ja050006u.

[11] W. A. A. Alhassan and I. A. Wadi. "Determination of Optical Energy Gap for Copper oxide at Different Temperatures." In: *International Journal of Advanced Engineering Research and Science* 5.3 (2018), pp. 255–258. DOI: 10.22161/ijaers.5.3.33. URL: https://doi.org/10.22161/ijaers.5.3.33.

[12] H. Liu. "Large-scale Synthesis of Cu2O Nanocubes and Their Electrochemical Properties." In: *International Journal of Electrochemical Science* (Apr. 2016), pp. 2756–2761. DOI: 10.20964/110402756. URL: https://doi.org/10.20964/110402756.

[13] T. Lan, A. Fallatah, E. Suiter, and S. Padalkar. "Size Controlled Copper (I) Oxide Nanoparticles Influence Sensitivity of Glucose Biosensor." In: *Sensors* 17.9 (Aug. 2017), p. 1944. DOI: 10.3390/s17091944. URL: https://doi.org/10.3390/s17091944.

[14] I. Acevedo-Restrepo, L. Blandón-Naranjo, J. Hoyos-Arbeláez, F. D. Pelle, and M. Vázquez. "Electrochemical Glucose Quantification as a Strategy for Ethanolic Fermentation Monitoring." In: *Chemosensors* 7.1 (Mar. 2019), p. 14. DOI: 10.3390/chemosensors7010014. URL: https://doi.org/10.3390/chemosensors7010014.

[15] K. Movlaee, M. Ganjali, P. Norouzi, and G. Neri. "Iron-Based Nanomaterials/Graphene Composites for Advanced Electrochemical Sensors." In: *Nanomaterials* 7.12 (Nov. 2017), p. 406. DOI: 10.3390/nano7120406. URL: https://doi.org/10.3390/nano7120406.

[16] W. Zheng, Y. Li, and L. Y. S. Lee. "Insights into the transition metal ion-mediated electrooxidation of glucose in alkaline electrolyte." In: *Electrochimica Acta* 308 (June 2019), pp. 9–19. DOI: 10.1016/j.electacta.2019.04.007. URL: https://doi.org/10.1016/j.electacta.2019.04.007.

[17] S. Marini, N. Ben Mansour, M. Hjiri, R. Dhahri, L. El Mir, C. Espro, A. Bonavita, S. Galvagno, G. Neri, and S. G. Leonardi. "Non-enzymatic Glucose Sensor Based on Nickel/Carbon Composite." In: *Electroanalysis* 30.4 (Jan. 2018), pp. 727–733. DOI: 10.1002/elan.201700687. URL: https://doi.org/10.1002/elan.201700687.

[18] J. Shi, D. Feng, and Y. Li. "Biosensors in Fermentation Applications." In: *Fermentation Processes*. InTech, Feb. 2017. DOI: 10.5772/65077. URL: https://doi.org/10.5772/65077.

[19] R. J. A. do Nascimento, G. R. de Macedo, E. S. dos Santos, and J. A. de Oliveira. "Real time and in situ Near-Infrared Spectroscopy (Nirs) for Quantitative Monitoring of Biomass, Glucose, Ethanol and Glycerine concentrations in an alcoholic fermentation." In: *Brazilian Journal of Chemical Engineering* 34.2 (Apr. 2017), pp. 459–468. DOI: 10.1590/0104-6632.20170342s20150347. URL: https://doi.org/10.1590/0104-6632.20170342s20150347.

[20] S. Leonardi, N. Donato, A. Bonavita, G. Neri, M. Bonyani, and A. Mirzaei. "Ag-doped nanostructured materials for electrochemical sensors." In: *2015 XVIII AISEM Annual Conference*. IEEE, Feb. 2015. DOI: 10.1109/aisem.2015.7066829. URL: https://doi.org/10.1109/aisem.2015.7066829.

[21] S. Leonardi, M. Bonyani, K. Ghosh, A. Dhara, L. Lombardo, N. Donato, and G. Neri. "Development of a Novel Cu(II) Complex Modified Electrode and a Portable Electrochemical Analyzer for the Determination of Dissolved Oxygen (DO) in Water." In: *Chemosensors* 4.2 (Apr. 2016), p. 7. DOI: 10.3390/chemosensors4020007. URL: https://doi.org/10.3390/chemosensors4020007.

[22] T. Denaro, V. Baglio, M Girolamo, G. Neri, F Deorsola, R Ornelas, F. Matteucci, V. Antonucci, and A S Aricò. "The Influence of Physico-Chemical Properties of Bare Titania Powders Obtained from Various Synthesis Routes on Their Photo-Electrochemical Performance." In: *International Journal of Electrochemical Science* 7 (Mar. 2012).

[23] F. Tavella, C. Ampelli, S. Leonardi, and G. Neri. "Photo-Electrochemical Sensing of Dopamine by a Novel Porous TiO2 Array-Modified Screen-Printed Ti Electrode." In: *Sensors* 18.10 (Oct. 2018), p. 3566. DOI: 10.3390/s18103566. URL: https://doi.org/10.3390/s18103566.

[24] N. Zahmouli, S. Marini, M. Guediri, N. B. Mansour, M. Hjiri, L. E. Mir, C. Espro, G. Neri, and S. Leonardi. "Nanostructured Nickel on Porous Carbon-Silica Matrix as an Efficient Electrocatalytic Material for a Non-Enzymatic Glucose Sensor." In: *Chemosensors* 6.4 (Nov. 2018), p. 54. DOI: 10.3390/chemosensors6040054. URL: https://doi.org/10.3390/chemosensors6040054.

[25] N. B. Mansour, M Hjiri, R Dahari, L. E. Mir, M Bonyani, A Mirzaei, S. G. Leonardi, and G Neri. "Synthesis, characterization and electrochemical properties of metal-doped nanoporous carbon." In: *IOP Conference Series: Materials Science and Engineering* 92 (Oct. 2015), p. 012005. DOI: 10.1088/1757-899x/92/1/012005. URL: https://doi.org/10.1088/1757-899x/92/1/012005.

[26] S. G. Leonardi, S. Marini, C. Espro, A. Bonavita, S. Galvagno, and G. Neri. "In-situ grown flower-like nanostructured CuO on screen printed carbon electrodes for non-enzymatic amperometric sensing of glucose." In: *Microchimica Acta* 184.7 (Apr. 2017), pp. 2375–2385. DOI: 10.1007/s00604-017-2232-1. URL: https://doi.org/10.1007/s00604-017-2232-1.

[27] Y. Wang, S. Lany, J. Ghanbaja, Y. Fagot-Revurat, Y. P. Chen, F. Soldera, D. Horwat, F. Mücklich, and J. F. Pierson. "Electronic structures ofCu2O, Cu4O3, and CuO: A joint experimental and theoretical study." In: *Physical Review B* 94.24 (Dec. 2016). DOI: 10.1103/physrevb.94.245418. URL: https://doi.org/10.1103/physrevb.94.245418.

[28] C. Lu, Z. Li, L. Ren, N. Su, D. Lu, and Z. Liu. "In Situ Oxidation of Cu2O Crystal for Electrochemical Detection of Glucose." In: *Sensors* 19.13 (July 2019), p. 2926. DOI: 10.3390/s19132926. URL: https://doi.org/10.3390/s19132926.

[29] Y. Zhao, L. Fan, Y. Zhang, H. Zhao, X. Li, Y. Li, L. Wen, Z. Yan, and Z. Huo. "Hyper-Branched Cu@Cu2O Coaxial Nanowires Mesh Electrode for Ultra-Sensitive Glucose Detection." In: *ACS Applied Materials & Interfaces* 7.30 (July 2015), pp. 16802–16812. DOI: 10.1021/acsami.5b04614. URL: https://doi.org/10.1021/acsami.5b04614.

Appendix A

Electrochemical Trials

Likewise in **(Chapter 5)** all the electrochemical tests performed for NC-9 and NC-10 samples were run with P25 and HS-1 samples. In fact **(Figure A.1)** reveal the results of all CV trials performed for all samples. Despite the similar behaviour of NC-10 and P25, probably lixing too, HS-1 show great results.

Both P25 and HS-1 samples oxidation reactions undergoes with diffusion control mass transfer. This can be easily visualize by the linear calibration curves varying the scan rate in CV setup shown at **(Figure A.2d and A.2f)**.

Despite the great current read in CV trials shown previously by the HS-1 sensor, this did not performed better than NC-9 sensor in amperommetry trials present in **(Figure A.3)**. Both calibration curves of this new samples have lower current values than NC-9 curves. Although HS-1 shown greater activity than P25 as in **(Figure A.3g)**.

All the samples performed good in selectivity tests as observed in **(Figure A.4)**. Although as refereed elsewhere the only sensor which was test with ethanol present in solution was NC-9, **(Figure A.4a)**.

Likewise selectivity test, repeatibility shown in **(Figure A.5)** was successfully reach by all modified electrodes. Despite the shift "rectangles"display in **(Figure A.5c and A.5d)** the standard deviation acquired really low values, which faces the really low current signal detected.

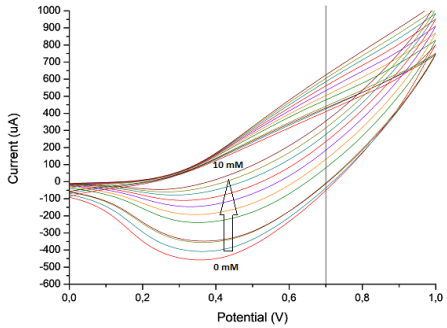

a) NC-9 cyclic voltammetry at 0.1 M KOH

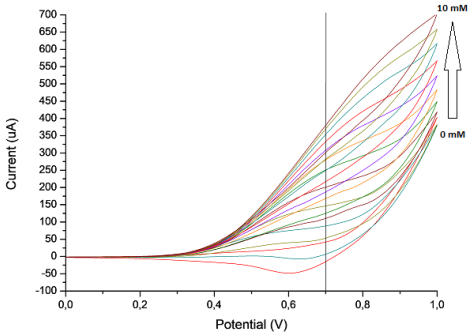

b) NC-10 cyclic voltammetry at 0.1 M KOH

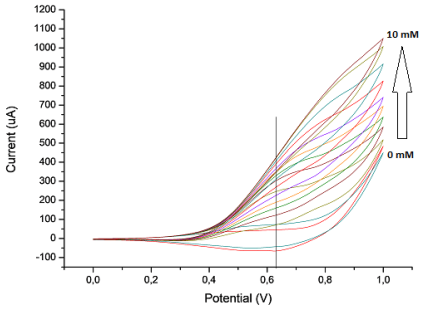

c) P25 cyclic voltammetry at 0.1 M KOH

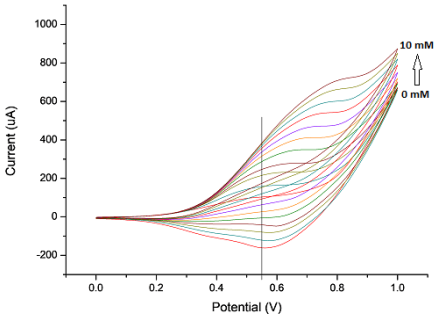

d) HS-1 cyclic voltammetry at 0.1 M KOH

Figure A.1: Cyclic voltammetry results for all samples at 0.1 M KOH

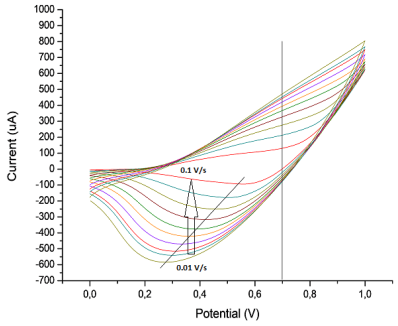

a) Cyclic voltammetry at different scan rate for sample NC-9 at 0.1 M KOH with 1 mM of glucose concentration

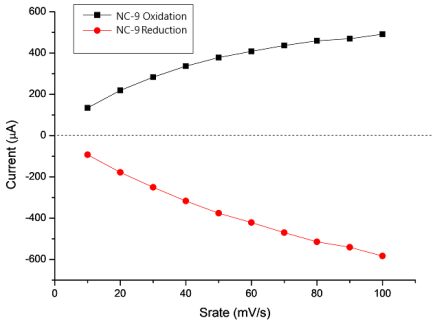

b) NC-9 Calibration curve at 0.1 M KOH with 1 mM of glucose concentration

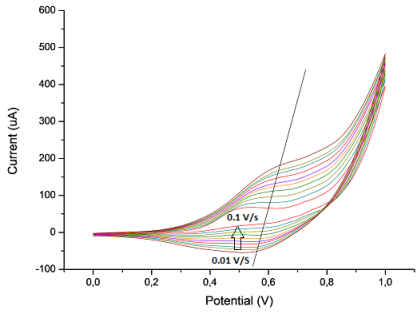

c) Cyclic voltammetry at different scan rate for sample P25 at 0.1 M KOH with 1 mM of glucose concentration

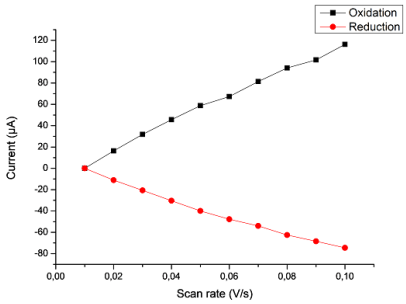

d) P25 Calibration curve at 0.1 M KOH with 1 mM of glucose concentration

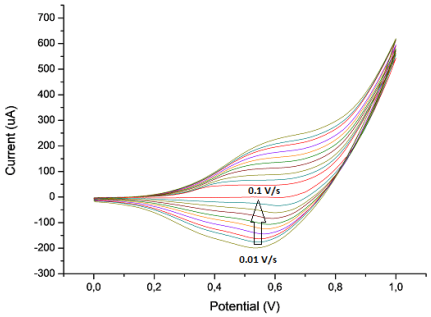

e) Cyclic voltammetry at different scan rate for sample HS-1 at 0.1 M KOH with 1 mM of glucose concentration

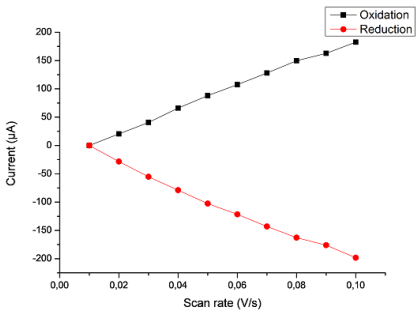

f) HS1 Calibration curve at 0.1 M KOH with 1 mM of glucose concentration

Figure A.2: Cyclic voltammetry at different scan rates results for all samples at 0.1 M KOH with 1 mM of glucose concentration

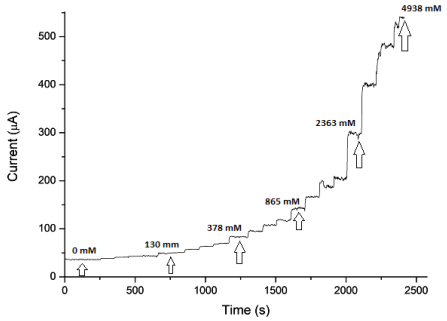

a) Chronoamperommetry for sample NC-9 at 0.7 V in 0.1 M KOH solution

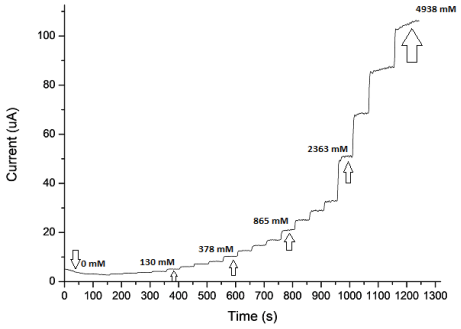

b) Chronoamperommetry for sample NC-10 at 0.7 V in 0.1 M KOH solution

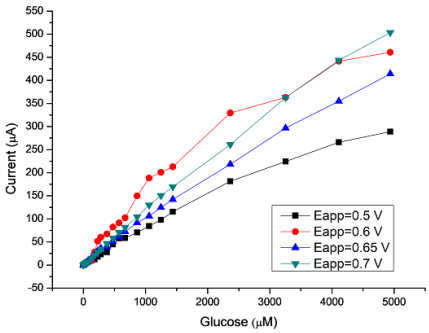

c) Calibration curve for sample NC-9 in 0.1 M KOH solution

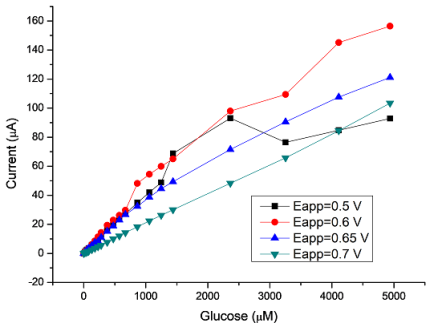

d) Calibration curve for sample NC-10 V in 0.1 M KOH solution

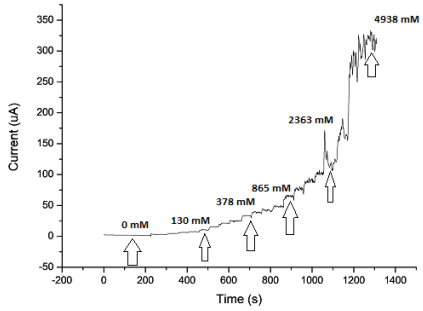

e) Chronoamperommetry for sample P25 at 0.7 V in 0.1 M KOH solution

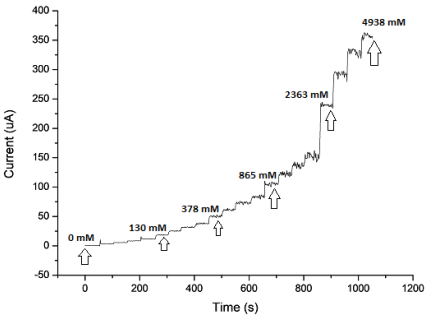

f) Chronoamperommetry for sample HS-1 at 0.7 V in 0.1 M KOH solution

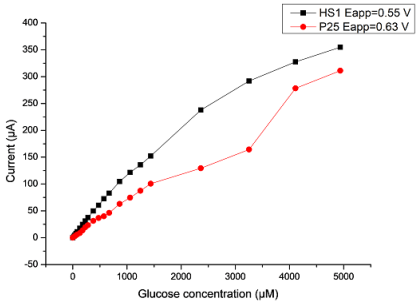

g) Calibration curve P25 vs HS-1 at 0.7 V in 0.1 M KOH solution

Figure A.3: Chronoamperommetry and calibration curves for all samples in 0.1 M KOH solution

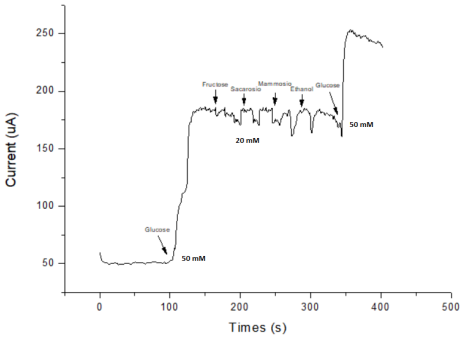

a) NC-9 selectivity test in 0.1 M KOH solution

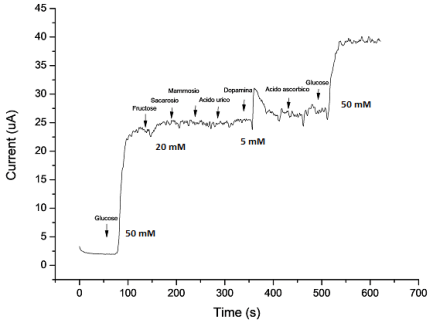

b) NC-10 selectivity test in 0.1 M KOH solution

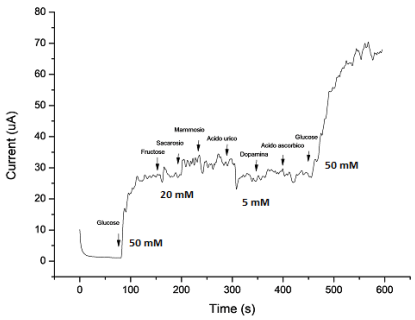

c) P25 selectivity test in 0.1 M KOH solution

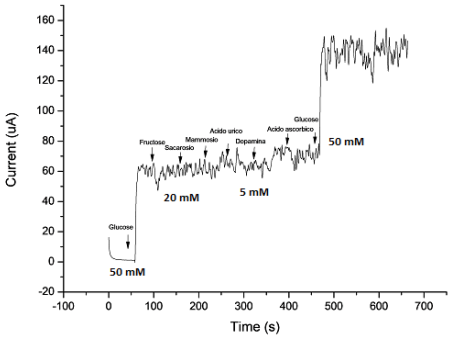

d) HS-1 selectivity test in 0.1 M KOH solution

Figure A.4: Selectivity results for all samples in 0.1 M KOH solution

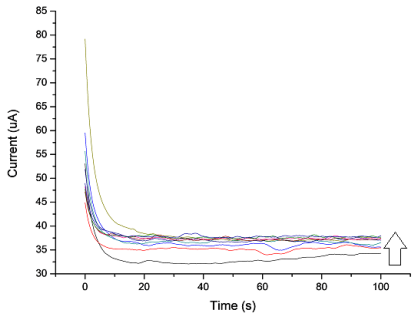

a) NC-9 repeatibility test in 0.1 M KOH solution

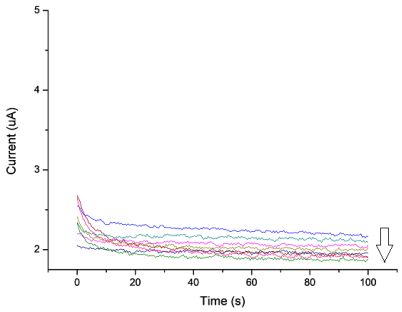

b) NC-10 repeatibility test in 0.1 M KOH solution

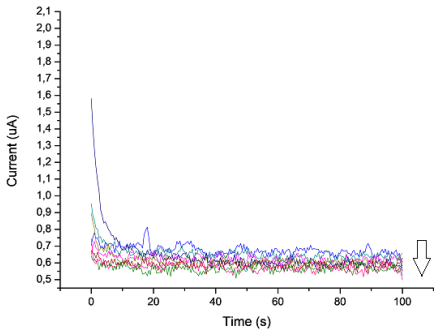

c) P25 repeatibility test in 0.1 M KOH solution

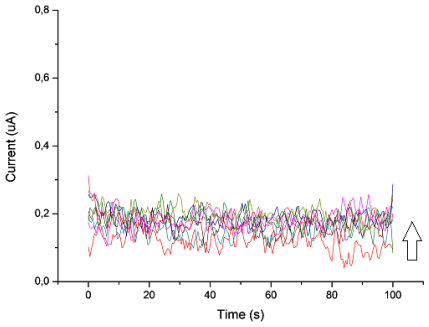

d) HS-1 repeatibility test in 0.1 M KOH solution

Figure A.5: Repeatibility results for all samples in 0.1 M KOH solution

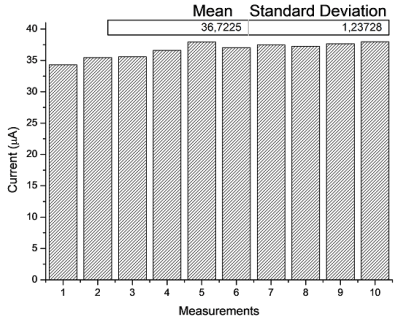

a) NC-9 repeatibility test mean and standard deviation in 0.1 M KOH solution

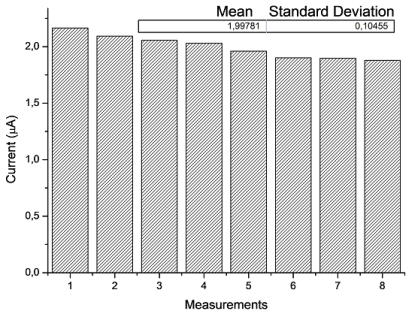

b) NC-10 repeatibility test mean and standard deviation in 0.1 M KOH solution

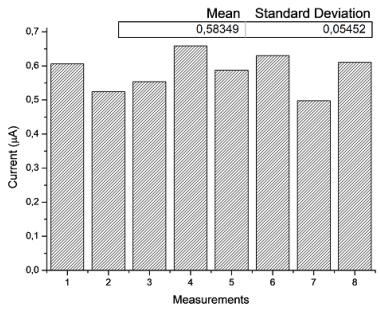

c) P25 repeatibility test mean and standard deviation in 0.1 M KOH solution

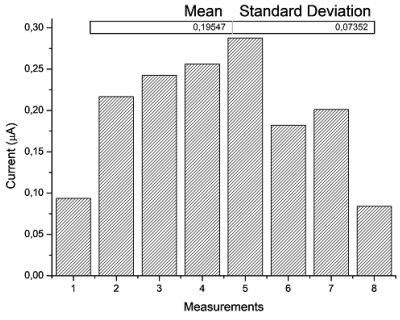

d) HS-1 repeatibility test mean and standard deviation in 0.1 M KOH solution

Figure A.6: Repeatibility test mean and standard deviation for all samples in 0.1 M KOH solution